

# Perturbation theory scope for predicting vibronic selectivity by entangled two photon absorption

C. D. Rodríguez-Camargo,<sup>1,\*</sup> H. Ó. Gestsson,<sup>1</sup> C. Nation,<sup>1</sup> A. R. Jones,<sup>2</sup> and A. Olaya-Castro<sup>1,†</sup>

<sup>1</sup>*Department of Physics and Astronomy, University College London, London WC1E 6BT, United Kingdom*

<sup>2</sup>*Biometrology, Department of Chemical and Biological Sciences, National Physical Laboratory, Teddington, Hampton Road, Middlesex TW11 0LW, United Kingdom*

Using second-order perturbation theory in the light-matter interaction, we derive an analytical approximation for the vibronic populations of a diatomic system excited by ultrabroadband frequency entangled photons and evaluate the population dynamics for different degrees of entanglement between photon pairs. Our analytical approach make the same predictions as previously derived via numerical solutions of the complete Schrödinger equation [H. Oka, *Physical Review A* 97, 063859 (2018)], with the added advantage of providing clear physical insights into the vibronic selectivity as a function of the degree of photon correlations while requiring significantly reduced computational effort. Specifically, our analytical expression for the probability of vibronic excitation includes a factor which predicts the enhancement of vibrational selectivity as a function of the degree correlation between the entangled photon pairs, the targeted vibrational energy level, and the vibrational molecular structure encoded in the Franck-Condon factors. Our results illustrate the importance of going beyond the usual approximations in second-order perturbation theory to capture the relevance of the vibrational structure of the molecular system of interest in order to gain a deeper understanding of the possible quantum-enhancement provided by the interaction between quantum light and matter.

## I. INTRODUCTION

Quantum entanglement is currently understood as a physical resource that can provide significant quantum advantages for a variety of processes and technologies, such as quantum teleportation [1, 2], quantum communication [3–5], cryptography [6], metrology [7–9], imaging [10–13], and sensing [14, 15]. In particular, entangled photon states have emerged as powerful and sensitive tools for probing complex molecular [16–18] and photo-sensitive biological systems [19–23].

Entangled two-photon absorption (ETPA) processes in molecular systems have been intensively investigated over the last decade [24–27]. In this process, the system transitions from the ground state to an excited state through the simultaneous absorption of a pair of entangled photons [24, 28, 29]. It has been proposed that quantum correlations embedded in the photon pair can provide an advantage in accessing molecular information which remains inaccessible to classical light sources [30, 31]. Indeed, a variety of quantum states of light can offer new avenues for selective molecular excitation as well as for controlling relaxation and radiative processes [27, 32, 33].

A prominent advantage of employing two-photon non-classical light in spectroscopy is the occurrence of a two-photon absorption process with a resonant intermediate state at a rate linearly proportional to the light flux [34–36]. For perfectly number-correlated light beams and low intensities, the flux of entangled photon pairs scales linearly with intensity, indicating that the biphoton effectively acts as a single unit [37]. For larger intensities, theory predicts a crossover between linear and quadratic dependence on the photon flux, the latter being characteristic of classical or uncorrelated two-photon absorption (CTPA) [38].

Several experimental efforts have been made to measure the ETPA cross sections of a variety of organic molecules [39–44], with discrepancies reported for the results from different laboratories performing measurements on the same molecular system [41, 45–47] and other experiments reporting no ETPA detection for the same set-up and system, where previous reports indicated positive results for ETPA absorption cross sections [41, 45]. For a comprehensive discussion of the bounds on ETPA absorption cross sections in common fluorophores and a detailed comparison between different experimental setups, we refer the reader to Ref. [47]. Hence, an open problem in the field is to understand the sources of experimental discrepancies and the inconsistencies between theory and experiment [45].

Most theoretical studies consider simplified models that do not necessarily capture the complexity of the systems of interest; for instance, they neglect the vibrational structure relevant to the systems [34, 48–52]. They also rely on perturbation approaches in limits that may not be compatible with the experimental conditions, for instance, finite-time pulses versus extended pulses [24, 34, 35, 53–55]. Indeed, it has been discussed that a more complete framework is necessary for a thorough understanding on the quantum advantage of ETPA [24, 56].

In particularly, considerations of the molecular electronic and vibrational structures of the systems of interest appear crucial for accurate predictions [57–60]. For instance, in Ref. [61] by studying zinc tetraphenylporphyrin (ZnTPP) molecule, it was shown that considering the details of the molecular electronic structure, it is possible to explain the spectral shifting between ETPA and CTPA measured in the experiments. The experimental and theoretical results of this study discern from previous theoretical descriptions which neglect the electronic or vibronic structure of the matter [51, 56, 62] and predicted similar shapes for ETPA and CTPA spectra.

A few numerical studies have considered the interaction between entangled photons pairs and molecular systems modeled with their relevant vibrational structures [57, 58, 63, 64].

\* christian.rodriguez-camargo.21@ucl.ac.uk

† a.olaya@ucl.ac.uk

In Ref. [64], the author considered a diatomic molecule with a vibrational structure in the intermediate and excited electronic states to investigate vibrational selectivity in the excited state via two-step excitation (TSE) by ultrabroadband frequency-entangled photons. The numerical approach employed relies on solving the complete Schrödinger equation, which requires large computational resources owing to the need for precise discretisation of the frequency domain of the entangled photon states and the large number of vibrational levels that need to be considered.

In this paper, we revise the findings of Ref. [64] and show that a carefully developed second-order perturbation theory that avoids common approximations, provides an efficient and insightful theoretical framework to investigate vibrational selectivity via ultra-broadband entangled photon pairs, as presented in [64]. Our approach significantly reduces the computational complexity of studying the interaction between the vibrational molecular structure and entangled photons, while providing clear physical insight into the factors dominating vibrational selectivity. Specifically, we derive a semi-analytical expression that predicts the population dynamics of the vibrational states in the excited electronic state for different degrees of correlation of the biphoton state. Our perturbative treatment assumes a finite-time light-matter interaction, without resorting to any in-resonance or far-resonance approximations. Using the same molecular parameters as those used in Ref. [64], we show that the dynamics predicted by our approach fully compare with the numerical solutions presented in [64] up to a small relative error, which decreases as the degree of entanglement increases.

Our analytical framework provides a clear understanding of how the excitation efficiency of vibronic excited states depends on the degree of photon correlation, the targeted vibrational energy level, and the molecular structure. We are therefore able to present a detailed analysis of the probability of transition from the ground to an excited vibronic state for intermediate degrees of photon correlations, not previously considered, and show that vibrational selectivity can be achieved for non-perfectly entangled pairs.

We also show how CTPA can be seen as a multiplicative single-photon process of transitions from ground to intermediate states, and from intermediate to excited states, while ETPA becomes a weighted average of two differentiated one-photon transitions, modulated by a Gaussian envelope that captures the resonance or off-resonance conditions and the degree of two-photon correlation. These results then allow us to understand the key physical differences in vibronic excitation with uncorrelated and quantum-correlated photons.

Taking advantage of the low computational effort required by our approach, we further explore different resonance scenarios to understand the selectivity properties of different vibrational levels in the excited electronic state, the number of entangled modes in the biphoton state, and the molecular structure. We discuss how the Franck-Condon structure is fundamental to understanding the differences that we observed, thereby highlighting the relevance of accounting for the vibronic structure of matter in predicting quantum enhancements given by entangled photon pairs, in line with re-

cent remarks [61].

The paper is organized as follows: In Sec. II we present the characterisation of the photon field and the molecular system. In Sec. III we present the interaction Hamiltonian, the perturbation theory approach and our analytical expression to evaluate the transition probabilities of interest, and establish the set of Schrödinger equations to be solved numerically to benchmark with [64]. In Sec. IV we present the comparison between the numerical approach and our analytical framework. Finally, in Sec. V we summarise our results and present the outlook and perspectives.

## II. THEORETICAL MODEL

In this section, we review the model and parameters presented in [64]. Hereafter, we use units such that  $\hbar = c = 1$ . Because we are developing an analytic structure to be compared with the numerical solutions of the complete Schrödinger equation, we do implement the same molecular parameters and simulation constants given in the aforementioned paper. First, we present the formalism involved in the configuration of frequency-entangled photons with energy anticorrelation. We present the one and two-photon states and their corresponding spectral amplitudes. We also present the molecular electronic-vibration configurations given by the Morse potentials and their vibrational eigenfunctions. Finally, we set the interaction Hamiltonian between the entangled photons and molecule given by the Franck-Condon approximation for transitions.

### A. Frequency-entangled photons with energy anticorrelation

We consider the interaction between two (propagating) pulses of a quantized radiation field (the “field” degrees of freedom) and three electronic energy levels of a molecule which has inner vibrational levels for each electronic level (the “molecular” degrees of freedom). In this section we describe the field Hamiltonian and its associated one-photon and two-photon states (uncorrelated and entangled).

The incoming light pulses impinge on the three-level target located at the origin of the reference frame (See Fig. 1). Each field is quantized within a (cylindrical) quantization volume, along the same propagation direction, giving rise to modes labeled by a one-dimensional continuous variable, either the wave vector  $k$  or frequency  $\omega$  [65]. Therefore, because we consider a one-dimensional input-output photon field interacting with a molecular system, we obtain annihilation  $\hat{a}(k)$ , and creation  $\hat{a}^\dagger(k)$  operators satisfying the commutation relation  $[\hat{a}(k), \hat{a}^\dagger(k')] = \delta(k - k')$ . In this framework, the total Hamiltonian for both fields is:

$$\hat{H}_F = \int dk k \hat{a}^\dagger(k) \hat{a}(k). \quad (1)$$

Since we are dealing with ultra-broadband photon fields, we avoid labels that differentiate signal and idler photons [66].

Within the field Hamiltonian (1) we define the one-photon state as [67, 68]

$$|\psi^{(1p)}\rangle = \int dk \psi^{(1p)}(k) \hat{a}^\dagger(k) |0\rangle, \quad (2)$$

where  $\psi^{(1p)}(k)$  is the momentum representation, or wave function, of the one-photon state  $|\psi^{(1p)}\rangle$  given by  $\psi^{(1p)}(k) = \langle k | \psi^{(1p)} \rangle$ , where  $|0\rangle$  is the vacuum state defined as is usual, i.e.,  $\hat{a}(k)|0\rangle = 0$ , and the continuous-mode single-photon state  $|k\rangle$  is defined by  $|k\rangle = |1_k\rangle = \hat{a}^\dagger(k)|0\rangle$  [65–69].

In an analogous way, we define the two-photon state as follows:

$$|\psi^{(2p)}\rangle = \int dk \int dk' \psi^{(2p)}(k, k') \hat{a}^\dagger(k) \hat{a}^\dagger(k') |0\rangle, \quad (3)$$

being  $\psi^{(2p)}(k, k') = \langle k, k' | \psi^{(2p)} \rangle$  the two-photon joint spectral amplitude (JSA) [70, 71].

The description of the two-photon JSA is provided by the definition of the spatiotemporal one-photon wave packet  $\varphi(r)$ . For simplicity, this wave packet can be described by a Gaussian form as follows [57]

$$\varphi(r) = \frac{1}{\sigma_r} \exp \left[ -\frac{(r - r_0)^2}{2\sigma_r^2} + ik_0(r - r_0) \right], \quad (4)$$

where  $r_0$  is the spatial center position of the wave packet at  $t_0$ ,  $\sigma_r$  is the coherent length of the wave packet, and  $k_0$  is the central energy of the photon pulse.

The one-photon wave packet in the  $k$  representation can be obtained using the Fourier transform of (4), which yields

$$\varphi(k) \exp(-ikr_0) = \frac{1}{\sqrt{2\pi}} \int_{-\infty}^{\infty} dr \varphi(r) \exp(-ikr). \quad (5)$$

Thus,

$$\varphi(k) = \frac{1}{\sqrt{2\sigma^2}} \exp \left[ -\frac{(k - k_0)^2}{4\sigma^2} \right] \quad (6)$$

where  $\sigma = \sigma_r^{-1}$  denotes the spectral width of the wave packet.

Using the one-photon wave packet, we can now describe the two-photon JSA  $\psi^{(2p)}(k, k')$ .

Since an uncorrelated photon pair has no correlation between the two photons, the two-photon joint amplitude can be expressed as the product of one-photon wave packets, given by [51]:

$$\psi_{unc}^{(2p)}(k, k') = \frac{1}{\sqrt{2\pi\sigma^2}} \varphi(k) \varphi(k') \exp[-i(k + k')r_0]. \quad (7)$$

On the other hand, the entangled photon pair with energy anticorrelation can be described as

$$\psi^{(2p)}(k, k') = \varphi(k) \delta(k + k' - 2k_0) \exp[-i(k + k')r_0]. \quad (8)$$

The Dirac delta function  $\delta(k + k' - 2k_0)$  ensures the quantum-mechanical energy anticorrelation of the two photons: one photon with energy  $k = k_0 - \Delta$  is accompanied by another photon with energy  $k' = k_0 + \Delta$ , conserving the total energy of  $2k_0$ . Using Fourier transform in the time domain, this property implies that the photon pair inherently has a time coincidence. Experimentally, this photon state can be obtained, i.e., by the spontaneous parametric down-conversion [72–74].

Generally, the energy anticorrelation of experimentally created entangled photons is not a Dirac delta, as shown in Eq. (8), but has a linewidth due to spontaneous emission. Here, we use the Gaussian definition of the Dirac delta function such that Eq. (8) is given by

$$\psi^{(2p)}(k, k') = \frac{1}{\sqrt{2\pi\sigma_s\sigma}} \varphi(k) \phi(k + k' - 2k_0) \exp[-i(k + k')r_0]. \quad (9)$$

where  $\phi(k)$  is defined as follows:

$$\phi(k) = \frac{1}{(\pi\sigma_s^2)^{1/4}} \exp\left(-\frac{k^2}{4\sigma_s^2}\right). \quad (10)$$

The function  $\phi(k)$  corresponds to the Dirac delta function in the limit of  $\sigma_s \rightarrow 0$ .

Note that expression (9) is not symmetric; thus, we shall work with a symmetrized version of this given by [56]

$$\psi_{sym}^{(2p)}(k, k') = \frac{\psi^{(2p)}(k, k') + \psi^{(2p)}(k', k)}{2}. \quad (11)$$

Remarking that throughout this paper, we shall follow the same parameters given in [64]; we set for the photon field  $\sigma = 10$  THz, and  $\sigma_s = 500$  GHz, as the upper bound in the correlation degree of entangled photons. We shall work with values of  $\sigma_s = \sigma$ ,  $\sigma_s = 0.5\sigma$ ,  $\sigma_s = 0.25\sigma$ ,  $\sigma_s = 0.1\sigma$ , and  $\sigma_s = 0.05\sigma$ .

To characterize the entanglement of correlated profiles, we use Schmidt decomposition [75–77]. This involves writing the JSA function  $\psi^{(2p)}(k, k')$  as a tensor product of two orthonormal sets  $\{|\phi\rangle_j\}$  and  $\{|\varphi\rangle_j\}$ , such that,

$$|\psi^{(2p)}(k, k')\rangle = \sum_j \lambda_j |\phi\rangle_j \otimes |\varphi\rangle_j, \quad (12)$$

which can similarly be written as,

$$\psi^{(2p)}(k, k') = \sum_j \lambda_j \phi_j(k) \varphi_j(k'), \quad (13)$$

where the coefficients  $\lambda_j$  are the so called Schmidt coefficients and  $\phi_j(k) \varphi_j(k')$  are the Schmidt modes [78].

The entanglement encoded in  $\psi^{(2p)}(k, k')$  can be quantified by the entanglement entropy [79, 80]

$$S = - \sum_j \lambda_j^2 \log_2 \lambda_j^2, \quad (14)$$

or Schmidt number given by

$$K = \frac{(\sum_j \lambda_j)^2}{\sum_j \lambda_j^2}. \quad (15)$$

In Fig. 1, in the part *a*), we depict a general form of a JSA (which is the fundamental object to characterize the propagating photon field) that departs from  $r = r_0 = -t_0$ , and interacts with the molecular system at  $r = 0$ . We also depict the first three contributions of the Schmidt decomposition, and expressions (14) and (15) for different correlation degrees. Note that the Schmidt number (15) increases significantly from  $\sigma_s = 0.1\sigma$ . This fact will help us to understand the selectivity dynamics derived from PT [61].

## B. Molecular system

We consider a molecular system (placed at  $r = 0$ ) which consists of three sets of vibronic states with inner vibrational modes: the ground state  $|g\rangle$ , the intermediate states  $\{|m_v\rangle\}_v$ , and the excited states  $\{|e_\alpha\rangle\}_\alpha$ . For the ground state, only the lowest vibrational mode was considered. The eigenenergies of these vibronic states are denoted as  $\omega_g, \omega_{m_v}, \omega_{e_\alpha}$ .

The molecular system is a diatomic molecule, for which we approximate the adiabatic potential curve using the Morse potential. Thus, it is possible to obtain the vibrational eigenfunctions analytically. See Fig. 1 part *b*). The Morse potential for the vibronic states of  $\ell$  is defined as [81, 82]:

$$V_\ell(x) = D_\ell \left[ \left( 1 - \exp\left(-\frac{x - x_0^\ell}{a_\ell}\right) \right)^2 - 1 \right], \quad (16)$$

where  $\ell$  is to label the levels  $g, m$ , and  $e$ ;  $x$  is the displacement of internuclear separation from the equilibrium position  $x_0$ .  $D$  and  $a$  are the depth and range of the potential, respectively. Therefore, the aforementioned eigenenergies of the vibronic states denoted by  $\omega_g, \omega_{m_v}, \omega_{e_\alpha}$  are given by:

$$\omega_{\ell_\beta} = \epsilon_\ell + \omega_\ell \left( \beta + \frac{1}{2} \right) - \omega_\ell \chi_\ell \left( \beta + \frac{1}{2} \right)^2, \quad (17)$$

where  $\epsilon_\ell$  is the minimum of the potential energy, and

$$\omega_\ell = \sqrt{\frac{2D_\ell}{a_\ell^2 \mu}} \quad (18)$$

with  $D_\ell$  and  $a_\ell$  are the depth and range of the potential, respectively. The expression for the anharmonicity of the Morse potential  $\chi_\ell$  is

$$\chi_\ell = \frac{1}{\sqrt{8a_\ell^2 D_\ell \mu}}. \quad (19)$$

Therefore, we shall adopt the following form for the molecular Hamiltonian

$$\hat{H}_{mol} = \sum_\alpha \omega_{e_\alpha} |e_\alpha\rangle \langle e_\alpha| + \sum_v \omega_{m_v} |m_v\rangle \langle m_v|. \quad (20)$$

Now, the corresponding vibrational eigenfunctions for each potential are given by

$$\xi_\beta^\ell(x) = N_{j_\ell, \beta} \exp(-y_\ell(x)/2) (y_\ell(x))^{j_\ell/2 - \beta} L_\beta^{j_\ell - 2\beta}(y_\ell(x)) \quad (21)$$

|                                 | $\epsilon_\ell$ | $D_\ell$  | $a_\ell$    | $x_0^\ell$ |
|---------------------------------|-----------------|-----------|-------------|------------|
| $ g\rangle$ ( $1^1\Sigma_g^+$ ) | 0 eV            | 0.7466 eV | $2.2951a_B$ | $5.82a_B$  |
| $ m\rangle$ ( $1^1\Sigma_u^+$ ) | 1.8201 eV       | 1.0303 eV | $3.6591a_B$ | $6.87a_B$  |
| $ e\rangle$ ( $2^1\Pi_g$ )      | 3.7918 eV       | 0.5718 eV | $3.1226a_B$ | $7.08a_B$  |

TABLE I. Morse parameters for the Na<sub>2</sub> molecule [84, 85]. Here  $a_B$  is the Bohr radius.  $\mu = 19800$  is used in the units of electron mass.

where  $L$  represents the generalized Laguerre polynomials, and

$$y_\ell(x) = (j_\ell + 1) \exp\left[\frac{-(x - x_0^\ell)}{a_\ell}\right], \quad (22)$$

being

$$j_\ell = 2a_\ell \sqrt{2\mu D_\ell} - 1. \quad (23)$$

The normalization constant is defined as

$$N_{j_\ell, \beta} = \left[ \frac{\beta! (j_\ell - 2\beta)!}{a_\ell \Gamma(j_\ell - \beta + 1)} \right]^{1/2}, \quad (24)$$

where  $\Gamma(z)$  denotes the gamma function.

For the optical transition, we adopt the Franck-Condon approximation. When the timescale of the light-molecule interaction is shorter than that of the molecular vibration, the optical transition rate between the two vibronic states can be approximated by the product of the electric-dipole transition rate and the Franck-Condon factor. The Franck-Condon factor is given by [83]

$$F_{\alpha v}^{\ell \ell'} = \left| \int dx \xi_v^{\ell'}(x) \xi_\alpha^\ell(x) \right|^2. \quad (25)$$

In this study, we use the Na<sub>2</sub> molecule as an example of a diatomic system. The Morse parameters are listed in the Table I. The Franck-Condon factors for this molecule are shown in the Fig. 1 part *c*) and *d*).

## C. Interaction Hamiltonian

Regarding the transitions, we consider only the transitions between  $|g\rangle$  and  $\{|m_v\rangle\}_v$ , and between  $\{|m_v\rangle\}_v$  and  $\{|e_\alpha\rangle\}_\alpha$ . Dashed arrows in Fig. 1 *b*). The direct transition from  $|g\rangle$  to  $\{|e_\alpha\rangle\}_\alpha$  by one photon, and the vibrational relaxations within  $\{|m_v\rangle\}_v$  and  $\{|e_\alpha\rangle\}_\alpha$  are ignored on the assumption of an ultra-cold molecule, for simplicity.

Thus, the Hamiltonian of the whole system is expressed as

$$\begin{aligned} \hat{H} = & \hat{H}_F + \hat{H}_{mol} \\ & + \sum_v \int dk \sqrt{\frac{\gamma_m F_{0v}^{gm}}{\pi}} (|m_v\rangle \langle g_0| \hat{a}(k) + \hat{a}^\dagger(k) |g_0\rangle \langle m_v|) \\ & + \sum_{v, \alpha} \int dk \sqrt{\frac{\gamma_e F_{v\alpha}^{me}}{\pi}} (|e_\alpha\rangle \langle m_v| \hat{a}(k) + \hat{a}^\dagger(k) |m_v\rangle \langle e_\alpha|), \end{aligned} \quad (26)$$

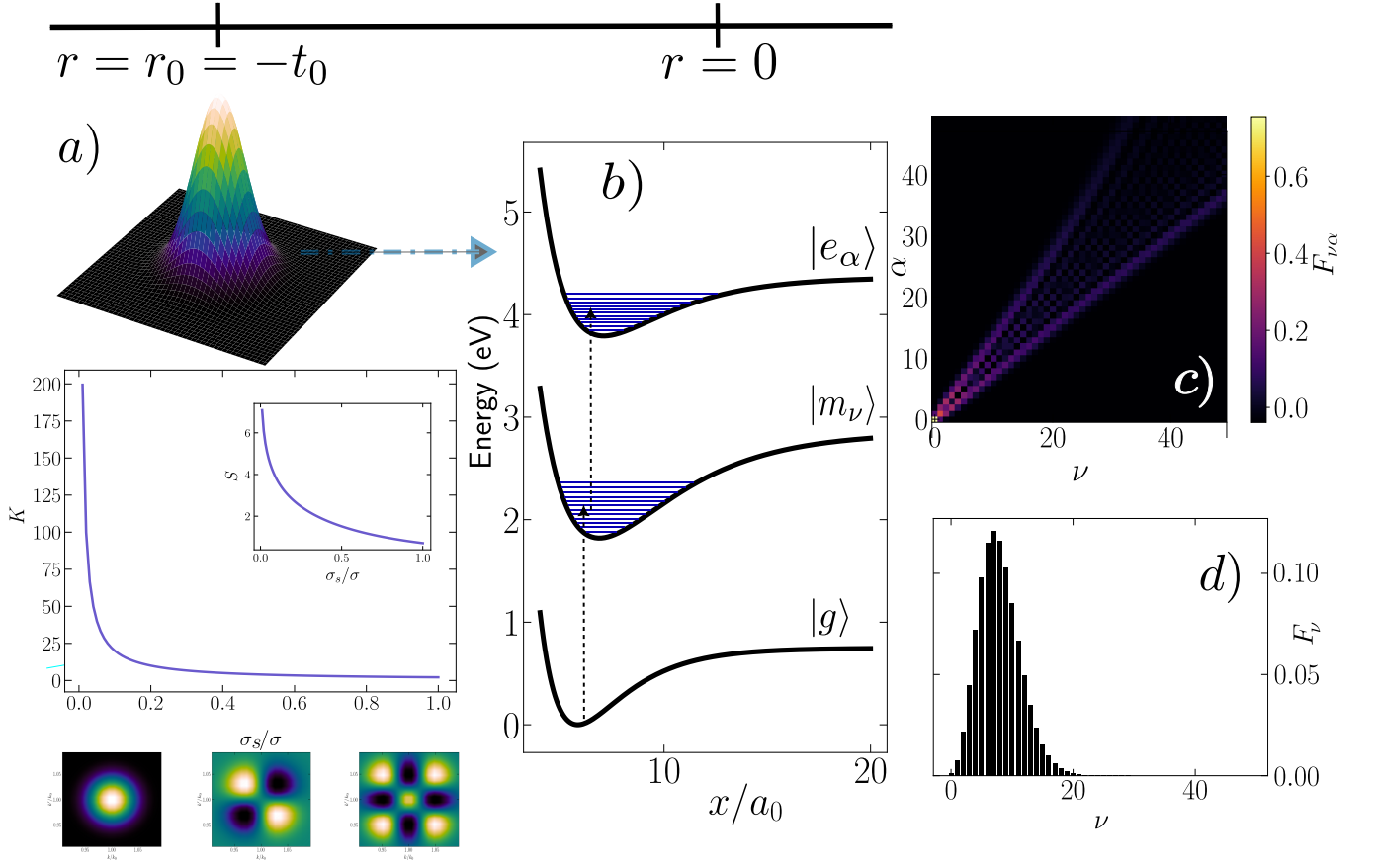


FIG. 1. Schematics of the physical system. *a)* A general form of a JSA which shall interact with the molecular system. The propagating photon field is departing from  $r = r_0 = -t_0$ . Below is depicted the Schmidt number (15) and the inset is describing the behaviour of the entanglement entropy (14). Below are depicted the three firsts contributions of the Schmidt decomposition of a JSA with  $\sigma_s = \sigma$ . These Schmidt modes are used to characterize the JSA and its Schmidt number and entropy. *b)* The three electronic levels of the molecular system, modeled by Morse potentials. The molecular system is placed at  $r = 0$ . The intermediate vibrational sublevels are labeled with  $\nu$ , while the excited vibrational sublevels are labeled by  $\alpha$ . We are considering transitions between the ground state  $|g\rangle$  and the intermediate sublevels  $\{|m_\nu\rangle\}_\nu$ , and between the intermediate sublevels  $\{|m_\nu\rangle\}_\nu$  and excited sublevels  $\{|e_\alpha\rangle\}_\alpha$ . These transitions are characterized by the Franck-Condon factors (25). The Franck-Condon factors  $F_{\nu\alpha}$  describing the transition from the intermediate sublevels and the excited sublevels are depicted in the part *c)*. The Franck-Condon factors  $F_{0\nu} \equiv F_\nu$  describing the transition from the ground state and the intermediate sublevels are depicted in the part *d)*.

where  $\gamma_{m_\nu}$  is the relaxation rate between  $|g\rangle$  and  $|m_\nu\rangle$  and  $\gamma_{e_{\nu\alpha}}$  is the relaxation rate between  $|m_\nu\rangle$  and  $|e_\alpha\rangle$ . In this study, we set  $\gamma = \gamma_{m_\nu} = \gamma_{e_{\nu\alpha}}$ . Under this assumption, the Hamiltonian (26) can be written as

$$\hat{H} = \hat{H}_F + \hat{H}_{mol} + \hat{H}_{int}, \quad (27)$$

where

$$\begin{aligned} \hat{H}_{int} = \gamma_s \left\{ \sum_\nu \int dk F_\nu [ |m_\nu\rangle \langle g | \hat{a}(k) + \hat{a}^\dagger(k) |g\rangle \langle m_\nu | ] \right. \\ \left. + \sum_{\nu,\alpha} \int dk F_{\nu\alpha} [ |e_\alpha\rangle \langle m_\nu | \hat{a}(k) + \hat{a}^\dagger(k) |m_\nu\rangle \langle e_\alpha | ] \right\}, \end{aligned} \quad (28)$$

with  $\gamma_s = \sqrt{\gamma}$ ,  $F_\nu = \sqrt{F_{0\nu}^{gm}/\pi}$  and  $F_{\nu\alpha} = \sqrt{F_{\nu\alpha}^{me}/\pi}$ .

### III. PERTURBATION THEORY AND QUANTUM DYNAMICS

In this section, we translate the Hamiltonian to the interaction picture, and we present the main result of this paper: the analytical expression for the vibrational populations derived from second order perturbation theory. Furthermore, we present the set of Schrödinger equations to be solved numerically, in order to compare the accuracy of our expression.

If we work within the interaction picture, we have

$$\hat{H}_{int}(t) = e^{i\hat{H}_0(t-t_0)} (\hat{H}_{int})_S e^{-i\hat{H}_0(t-t_0)}, \quad \hat{H}_0 = \hat{H}_F + \hat{H}_{mol}, \quad (29)$$

which yields

$$\hat{H}_{int}(t) = \gamma_s \left\{ \sum_\nu F_\nu \hat{\tau}_\nu(t) + \sum_{\nu,\nu'} F_{\nu\nu'} \hat{\tau}_{\nu\nu'}(t) \right\}. \quad (30)$$

If the light-matter interaction is switched on at  $t = -t_0$ , the

operators  $\hat{\tau}_v(t)$  and  $\hat{\tau}_{v'}(t)$  have the following form

$$\hat{\tau}_v(t) = e^{i\omega_{m_v}(t+t_0)}|m_v\rangle\langle g|\hat{a}(t) + e^{-i\omega_{m_v}(t+t_0)}\hat{a}^\dagger(t)|g\rangle\langle m_v|, \quad (31)$$

and

$$\begin{aligned} \hat{\tau}_{v'}(t) &= e^{i(\omega_{e_{v'}} - \omega_{m_v})(t+t_0)}|e_{v'}\rangle\langle m_v|\hat{a}(t) \\ &+ e^{-i(\omega_{e_{v'}} - \omega_{m_v})(t+t_0)}\hat{a}^\dagger(t)|m_v\rangle\langle e_{v'}|. \end{aligned} \quad (32)$$

In order to apply these operators, we can define an initial state as

$$|\psi_0\rangle = |\varphi_0\rangle \otimes |g\rangle, \quad (33)$$

where  $|\varphi_0\rangle$  is the initial state of the field and  $|g\rangle$  ground state of the molecule.

Using a perturbative expansion, the evolution operator satisfies

$$\begin{aligned} \hat{U}(t, t_0) &= 1 - i \int_{-t_0}^t dt' \hat{H}_{\text{int}}(t') \\ &+ (-i)^2 \int_{-t_0}^t dt' \hat{H}_{\text{int}}(t') \int_{-t_0}^{t'} dt'' \hat{H}_{\text{int}}(t''). \end{aligned} \quad (34)$$

Therefore, the transition between state  $|g, \psi_{2p}\rangle$ , which is the molecular ground state and the entangled pair of photons, to state  $|e_\alpha, 0\rangle$ , which is the vibrational excited state  $\alpha$  and the vacuum in the field, is given by

$$\langle e_\alpha, 0|\hat{U}(t, t_0)|g, \psi_{2p}\rangle = (-i\gamma_s)^2 \int_{-t_0}^t dt' \int_{-t_0}^{t'} dt'' \sum_y G_{v\alpha}(t', t''), \quad (35)$$

where

$$G_{v\alpha}(t', t) = F_v F_{v\alpha} \exp[i\Omega_{\alpha v}(t' + t_0) + i\omega_{m_v}(t'' + t_0)] \phi_q(t, t'), \quad (36)$$

with  $\Omega_{\alpha v} = \omega_{e_\alpha} - \omega_{m_v}$ , and

$$\phi_q(t, t') = \langle 0|\hat{a}(t)\hat{a}(t')|\psi_{2p}\rangle \quad (37)$$

is the so-called two-photon wavefunction [37].

After some algebraic manipulations, Eq. (35) reads

$$\langle e_\alpha, 0|\hat{U}(t, t_0)|g, \psi_{2p}\rangle = 2(-i\gamma_s)^2 \sum_y F_v F_{v\alpha} T_{v\alpha}(t, t_0), \quad (38)$$

where

$$T_{v\alpha}(t, t_0) = \int_{-t_0}^t dt' \int_{-t_0}^{t'} dt'' \int dk \int dk' \exp[-i(k' - \Omega_{\alpha v})(t' + t_0) - i(k - \omega_{m_v})(t'' + t_0)] \psi_{\text{sym}}(k, k'), \quad (39)$$

being  $\psi_{\text{sym}}(k, k')$  the symmetrized form of the JSA of the entangled photons.

Since we are in the regime in which the incoming photon pulses of bandwidth  $\Delta k$  are much smaller than their central frequency  $k_0$ , we extend the range of all the above frequency integrals to  $(-\infty, \infty)$ , such that, Eq. (39) reads

$$\begin{aligned} T_{v\alpha}(t, t_0) &= - \int_{-\infty}^{\infty} dk \int_{-\infty}^{\infty} dk' \frac{\exp[-i(k + k' - \omega_{e_\alpha})t] \psi_{\text{sym}}(k, k')}{(k - \omega_{m_v})(k + k' - \omega_{e_\alpha})} - \int_{-\infty}^{\infty} dk \int_{-\infty}^{\infty} dk' \frac{\exp[-i(k + k' - \omega_{e_\alpha})t_0] \psi_{\text{sym}}(k, k')}{(k' - \omega_{e_\alpha} + \omega_{m_v})(k + k' - \omega_{e_\alpha})} \\ &+ \int_{-\infty}^{\infty} dk \int_{-\infty}^{\infty} dk' \frac{\exp[-i(k' - \omega_{e_\alpha} + \omega_{m_v})t + (k - \omega_{m_v})t_0] \psi_{\text{sym}}(k, k')}{(k - \omega_{m_v})(k' - \omega_{e_\alpha} + \omega_{m_v})}. \end{aligned} \quad (40)$$

In the case of uncorrelated photons, we use the expression (7), such that Eq. (38) yields

$$\langle e_\alpha, 0|\hat{U}(t, t_0)|g, \psi_{2p}\rangle = \frac{\pi \sqrt{\pi}(-i\gamma_s)^2}{\sqrt{2\sigma^2}} \exp(i\omega_{e_\alpha} t) \sum_y F_v F_{v\alpha} \zeta_{v\alpha}^{(u)} \left\{ \varrho_{v\alpha}^{(u)}(t, t_0) + I_{v\alpha}^{(u)}(t, t_0) \right\}, \quad (41)$$

being

$$\zeta_{v\alpha}^{(u)} = \exp\left[-\frac{(k_0 - \omega_{m_v})^2}{4\sigma^2} - \frac{(k_0 - \Omega_{\alpha v})^2}{4\sigma^2}\right], \quad (42)$$

$$\begin{aligned} \varrho_{v\alpha}^{(u)}(t, t_0) &= \text{erfi}\left(i\sigma(t - t_0) + \frac{1}{2\sigma}(k_0 - \Omega_{\alpha v})\right) \left[ 2 \text{erf}\left(\sigma(t - t_0) - \frac{i}{2\sigma}(k_0 - \omega_{m_v})\right) - \text{erf}\left(2\sigma t - \frac{i}{2\sigma}(k_0 - \omega_{m_v})\right) \right] \\ &- \text{erfi}\left(2i\sigma t + \frac{1}{2\sigma}(k_0 - \Omega_{\alpha v})\right) \text{erf}\left(2\sigma t - \frac{i}{2\sigma}(k_0 - \omega_{m_v})\right) \end{aligned} \quad (43)$$

and

$$I_{v\alpha}^{(u)}(t, t_0) = \frac{i}{\pi\sigma^2} \sum_{n,l=0}^{\infty} \frac{(-1)^l \sigma^{-2(n+l)}}{2^{n+l} n! l! (2l+1)} \left[ 2t^2 \sigma^4 f_{n,l}^{(u,1)}(t, t_0) + \frac{2t\sigma^2 - i(k_0 - \omega_{m_v})}{(2n+1)(\omega_{e_\alpha} - 2\omega_{m_v})} f_{n,l}^{(u,2)}(t, t_0) \right], \quad (44)$$

where  $\text{erf}(z)$  is the error function of the complex variable  $z$  defined as,

$$\text{erf}(z) = \frac{2}{\sqrt{\pi}} \int_0^z dt \exp(-t^2), \quad (45)$$

$\text{erfi}(z)$  is the imaginary error function given by  $\text{erfi}(z) = -i \text{erf}(iz)$ , and the explicit forms of  $f_{n,l}^{(u,1)}(t, t_0)$  and  $f_{n,l}^{(u,2)}(t, t_0)$  are given in the Appendix.

The expression (41) describes the product of two Gaussians, which envelop a function composed of the product of the error functions. The first Gaussian function is centered at the resonance of the intermediate state energies and half of the central energy,  $k_0$ . One may observe that this part accounts for one-photon processes from the ground state to intermediate states. The second term is centered where the difference in energies between excited and intermediate states, that is,  $\Omega_{av}$  is in resonance with half of the central energy,  $k_0$ . Therefore, this structure is describing one-photon processes which occur between intermediate and excited states.

To obtain an expression for the transition amplitude of correlated photons, we use Eqs. (9) and (11) to define  $\psi_{sym}(k, k')$ , such that the symmetrized form reads

$$\psi_{sym}(k, k') = \frac{1}{2\sqrt{2\pi\sigma_s\sigma N}} \phi(k + k' - 2k_0) \exp[-i(k + k')r_0] \{\varphi(k) + \varphi(k')\}, \quad (46)$$

where we have introduced a normalization factor  $N$  given by

$$N = \sqrt{\frac{1}{2} + \frac{\sigma}{\sqrt{4\sigma^2 + \sigma_s^2}}}, \quad (47)$$

in order to have  $\int \int dk dk' |\psi_{sym}(k, k')|^2 = 1$ . After some manipulations, Eq. (38) yields

$$\langle e_\alpha, 0 | \hat{U}(t, t_0) | g, \psi_{2p} \rangle = \frac{\pi \sqrt{\pi} (-i\gamma)^2}{2\sqrt{2\sigma\sigma_s N}} \exp(i\omega_{e_\alpha} t) \zeta_\alpha \sum_\nu F_\nu F_{\nu\alpha} \left\{ \exp\left[-\frac{(k_0 - \omega_{m_\nu})^2}{4\sigma^2}\right] \rho_{\nu\alpha}^{(en,1)}(t, t_0) + \exp\left[-\frac{(k_0 - \Omega_{av})^2}{4\sigma^2}\right] \rho_{\nu\alpha}^{(en,2)}(t, t_0) \right\}, \quad (48)$$

where

$$\zeta_\alpha = \exp\left[-\frac{(2k_0 - \omega_{e_\alpha})^2}{4\sigma_s^2}\right], \quad (49)$$

$$\rho_{\nu\alpha}^{(en,1)}(t, t_0) = \text{erf}\left(\frac{i}{2\sigma}(k_0 - \omega_{m_\nu})\right) \left[ \text{erf}\left(2\sigma_s t - \frac{i}{2\sigma_s}(2k_0 - \omega_{e_\alpha})\right) - \text{erf}\left(\sigma_s(t - t_0) - \frac{i}{2\sigma_s}(2k_0 - \omega_{e_\alpha})\right) \right] + I_{\nu\alpha}^{(en,1)}(t, t_0), \quad (50)$$

and

$$\rho_{\nu\alpha}^{(en,2)}(t, t_0) = \text{erfi}\left(\frac{-2i\sigma^2\sigma_s^2(t - t_0) - \sigma^2(2k_0 - \omega_{e_\alpha}) - \sigma_s^2(k_0 - \Omega_{av})}{2\sigma\sigma_s\sqrt{\sigma^2 + \sigma_s^2}}\right) \left[ (i + 1) \text{erf}\left(\frac{2\sigma_s^2(t - t_0) - i(k_0 - \omega_{m_\nu})}{2\sqrt{\sigma^2 + \sigma_s^2}}\right) \right] + I_{\nu\alpha}^{(en,2)}(t, t_0). \quad (51)$$

In this case, we can observe a clear separation between the excitation processes from the ground states to the intermediate states, and the excitation processes from the intermediate states to the excited states. However, both are weighted by the product of the Franck-Condon factors from the ground to intermediate levels  $\nu$ ,  $F_\nu$ , and the Franck-Condon factors from intermediate levels  $\nu$ , to excited levels  $\alpha$ ,  $F_{\nu\alpha}$ , and a Gaussian function centered at the resonance between the target level eigenenergy and the correlated photons central energy  $2k_0$ , defined by Eq. (49). See Fig. 2. Within this fact, we may evidence that second-order PT predicts the strongly enhanced vibrational-mode-selective two-step excitation by ultrabroad-

band frequency-entangled photons, and provides a function to control in a more precise way this vibrational selectivity at the experimental level with other kinds of molecular systems. Notice that by maintaining the integrals in Eq. (39) at a finite temporal interval, gives us information about memory processes weighted by the spectral width of the wave packet, and the correlation parameter  $\sigma_s$ , given in the terms  $\sigma(t + t_0)$  and  $\sigma_s(t - t_0)$ . Furthermore, the structures of the arguments of the error functions provide information on the relationships that arise between the photons correlations and vibronic correlations. The explicit forms of expressions (44), (50), and

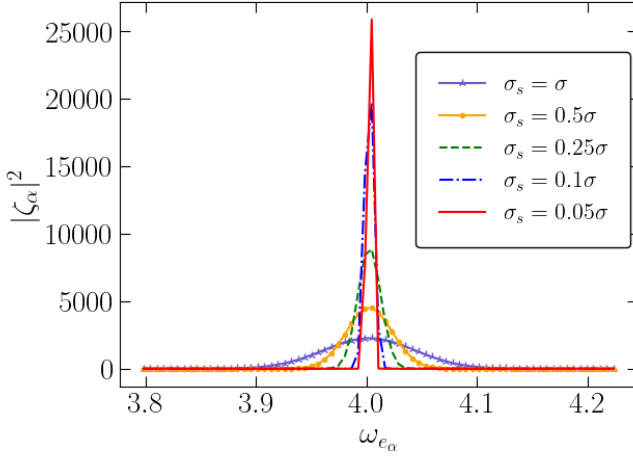


FIG. 2. Envelope Gaussian function which establish selectivity.

(51) can be found in the Appendix C.

### 1. Quantum dynamics

To compare the results from Perturbation Theory, we solve numerically the complete Schrödinger equation

$$\frac{d}{dt}|\Psi(t)\rangle = -i\hat{H}|\Psi(t)\rangle, \quad (52)$$

where  $|\Psi(t)\rangle$  is a superposition state given by

$$\begin{aligned} |\Psi(t)\rangle &= \frac{1}{\sqrt{2}} \int dk \int dk' \psi_{sym}^{(2p)}(k, k', t) \hat{a}^\dagger(k) \hat{a}^\dagger(k') |0\rangle |g_0\rangle \\ &+ \sum_\nu \int dk \psi^{(1pm)}(k, \nu, t) \hat{a}^\dagger(k) |0\rangle |m_\nu\rangle \\ &+ \sum_{\nu'} \psi^{(e)}(\nu', t) |0\rangle |e_{\nu'}\rangle, \end{aligned} \quad (53)$$

where  $\psi_{sym}^{(2p)}(k, k', t)$  is the two-photon joint amplitude of the incident pulse at  $|g_0\rangle$ ,  $\psi^{(1pm)}(k, \nu, t)$  is the one-photon state at  $|m_\nu\rangle$ , and  $\psi^{(e)}(\nu', t)$  is the zero-photon state at  $|e_{\nu'}\rangle$ .

For simplicity, in the calculation of quantum dynamics, we omit the degrees of freedom of the polarization of light by assuming linearly polarized light.

Applying the Hamiltonian operator to state (53), we obtain the following set of Schrödinger equations:

$$\begin{aligned} \frac{d}{dt} \psi_{sym}^{(2p)}(k, k', t) &= -i(k + k') \psi_{sym}^{(2p)}(k, k', t) \\ &- i\gamma_s \sum_\nu \frac{1}{\sqrt{2}} F_\nu [\psi^{(1pm)}(k, \nu, t) \\ &+ \psi^{(1pm)}(k', \nu, t)], \end{aligned} \quad (54)$$

$$\begin{aligned} \frac{d}{dt} \psi^{(1pm)}(k, \nu, t) &= -i(k + \omega_{m_\nu}) \psi^{(1pm)}(k, \nu, t) \\ &- i\gamma_s \sqrt{2} F_\nu \int dk' \psi_{sym}^{(2p)}(k, k', t) \\ &- i\gamma_s \sum_\alpha F_{\nu\alpha} \psi^{(e)}(\alpha, t), \end{aligned} \quad (55)$$

$$\begin{aligned} \frac{d}{dt} \psi^{(e)}(\alpha, t) &= -i\omega_{e_\alpha} \psi^{(e)}(\alpha, t) \\ &- i\gamma_s \sum_\nu F_{\nu\alpha} \int dk \psi^{(1pm)}(k, \nu, t). \end{aligned} \quad (56)$$

The initial state of the whole system is given by  $\psi^{(1pm)}(k, \nu, 0) = \psi^{(e)}(\alpha, 0) = 0$ .

In order to solve Eqs. (54), (55), and (56), we discretize the photon fields by converting from  $\int dk$  to  $\sum_k \delta k$ , and  $\hat{a}(k)$  to  $\hat{a}_k$ , and set  $\delta k = 100$  GHz. We refer the reader to Appendix A for a detailed description of the discretized Schrödinger equations.

## IV. POPULATION DYNAMICS

In this section, we analyze the temporal behavior of Eqs. (41) and (48), and we compare them with the numerical solutions of Eqs. (54), (55), and (56). Recall that the central energy of the entangled photons is set to  $2k_0 = \omega_{e_{\alpha=18}} \approx 4.0024$  eV, and  $\gamma = 6$  MHz. We define  $\langle e_\nu \rangle = |\langle e_\nu, 0 | \hat{U}(t) | g, \psi_{2p} \rangle|^2$ .

In Fig. 4, we depict the results for the uncorrelated JSA (7), and low entanglement degrees  $\sigma_s = \sigma$ , and  $\sigma_s = 0.5\sigma$ . In Fig. 5, we plot for the JSA with entanglement degrees  $\sigma_s = 0.25\sigma$ ,  $\sigma_s = 0.1\sigma$ , and the most entangled degree  $\sigma_s = 0.05\sigma$ . In all the Figures, the first column corresponds to the visualization of the JSA. The second column presents the results obtained by numerically solving Eqs. (54), (55), and (56). In the third column we depict Eqs. (41) and (48).

For uncorrelated photons, our expression predicts the simultaneously exciting of many vibrational modes owing to short pulse excitation with a spectrally broad bandwidth. The same phenomena were obtained using the numerical method. In addition, our expression reproduces the order (in terms of the numerical value achieved in the steady state) of the depicted levels. We can see that the differences between PT and the numerical method, in general, are given by: i) The slope of the transition between the null population value and steady state. For all levels, is higher for our expression; ii) Our expression reproduces the formation of Gaussian peaks in the neighborhood of  $r\sigma = 0$  (where the molecular system is placed), for all levels. However, there is a substantial difference between the numerical results given by the narrowing, and the maximum values. In addition, for the maximum population, achieved for  $\alpha = 12$ , we observed the occurrence of a small Gaussian peak that was not observed in the numerical results.

In Ref. [64] it is observed that the maximum population is achieved for  $\alpha = 12$  owing to the value of the Franck-Condon



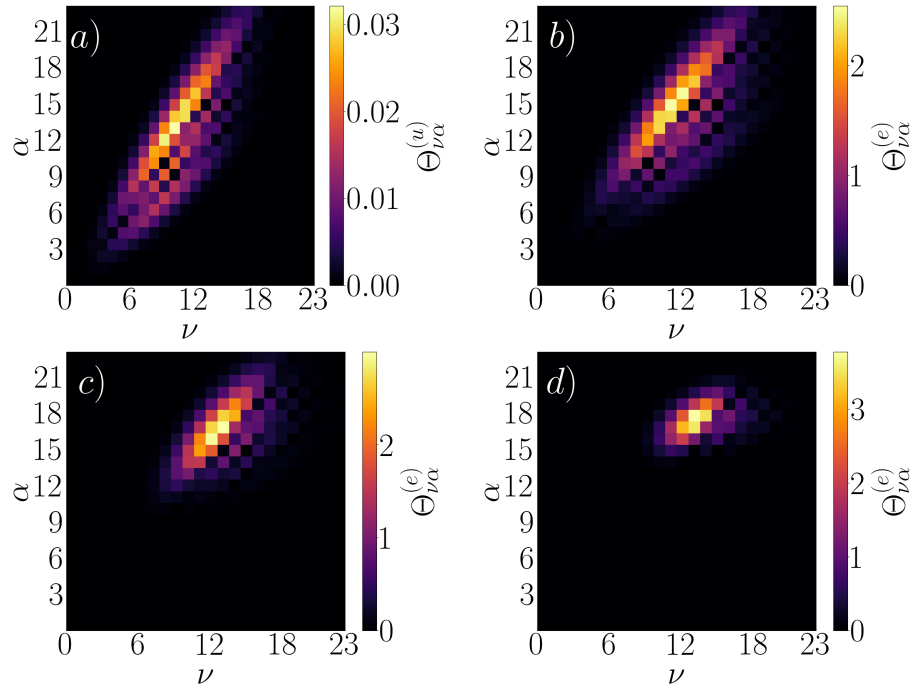


FIG. 3. Behaviour the transition matrices  $\Theta_{\mu\alpha}^{(u,e)}$  as a function of the correlation degree. *a)* The transition matrix  $\Theta_{\mu\alpha}^{(u)}$ . The transition matrix  $\Theta_{\mu\alpha}^{(e)}$  with: *b)*  $\sigma_s = \sigma$ , *c)*  $\sigma_s = 0.5\sigma$ , and *d)*  $\sigma_s = 0.25\sigma$ . Compare with the maximum values achieved in Figs. 4 and 5.

factors  $F_{\nu,\alpha=18}$ , which are very small for  $\nu < 12$ , and  $F_{\nu=10,\alpha=12}$  becomes larger. For  $\sigma_s = \sigma$  we have that the maximum population is now achieved for  $\alpha = 14$ , followed by  $\alpha = 16$ , and  $\alpha = 15$ .

Since the correlation between the photons is low, we have simultaneous excitations, as in the classical situation. This can be explained by the structure of Eqs. (41) and (48), respectively. The Gaussian structure of Eq. (48) is now dominated by Eq. (49). For higher  $\sigma_s$ , this factor has a broad form, which allows simultaneous excitations. However, the factor is pushing towards to the targeted level, supported by the Gaussians shaped by the spectral width of the wave packet  $\sigma$  and the energy differences  $(k_0 - \omega_{m_\nu})$  and  $(k_0 - \Omega_{\alpha\nu})$ , which could be encoded in an *effective* entangled transition factor defined by

$$\zeta_{\nu\alpha}^{(e)} = \zeta_\alpha \left\{ \exp \left[ -\frac{(k_0 - \omega_{m_\nu})^2}{4\sigma^2} \right] + \exp \left[ -\frac{(k_0 - \Omega_{\alpha\nu})^2}{4\sigma^2} \right] \right\}. \quad (57)$$

To illustrate this point, let us define the transition matrix elements  $\Theta_{\mu\alpha}^{(u,e)}$  as

$$\Theta_{\nu\alpha}^{(u,e)} = F_\nu F_{\nu\alpha} \zeta_{\nu\alpha}^{(u,e)}. \quad (58)$$

In Fig. 3, we plot the matrix elements (58) for the uncorrelated, and correlated cases. Panel *a)* shows the uncorrelated case. Panels *b)*, *c)*, *d)*, show  $\sigma_s = \sigma$ ,  $\sigma_s = 0.5\sigma$ , and  $\sigma_s = 0.25\sigma$ , respectively. We can evidence the displacement of the maximum achieved in the CTPA to the maximum achieved to each  $\sigma_s = \sigma$ -ETPA predicted using Eq. (57). Furthermore, notice the maximum values in each panel; our factor

predicts (and can quantify) the quantum enhancement of the ETPA.

For  $\sigma_s = 0.5\sigma$ , the levels near to the resonance, that is,  $\alpha = 17$  and  $\alpha = 16$ , achieve the maximum population. This is due to the fact that the factor Eq. (49) becomes narrower. We can also observe that the three main differences mentioned above are still present.

For  $\sigma_s = 0.25\sigma$ , the maximum population is achieved by the targeted level, followed by levels near the resonance  $\alpha = 17$ , and  $\alpha = 19$ . Other levels with a significant population were  $\alpha = 16$ , and  $\alpha = 20$ . This means that the factor (49) becomes dominant. In this framework, for  $\sigma_s = 0.1\sigma$ , the targeted level achieved a dominant contribution, and for  $\sigma_s = 0.05\sigma$ , the targeted level was completely selected, with a significant increase in the numerical value with respect to the other correlation degrees.

In Fig. 6, we depict the evolution of the targeted level with respect to the increase in the degree of correlation between photons. The first issue to be noted, is that our expression matches the results obtained using the numerical method. The separation between each steady state differed only in the uncorrelated case. The gap between the correlation degrees can be explained in terms of what is shown in Fig. 1 *a)*. Recall that from  $\sigma_s \approx 0.2\sigma$ , the Schmidt number begins to increase significantly as  $\sigma_s \rightarrow 0$ . That is, we have more entangled modes participating in the ETPA. This physical information is encoded in Eq. (49).

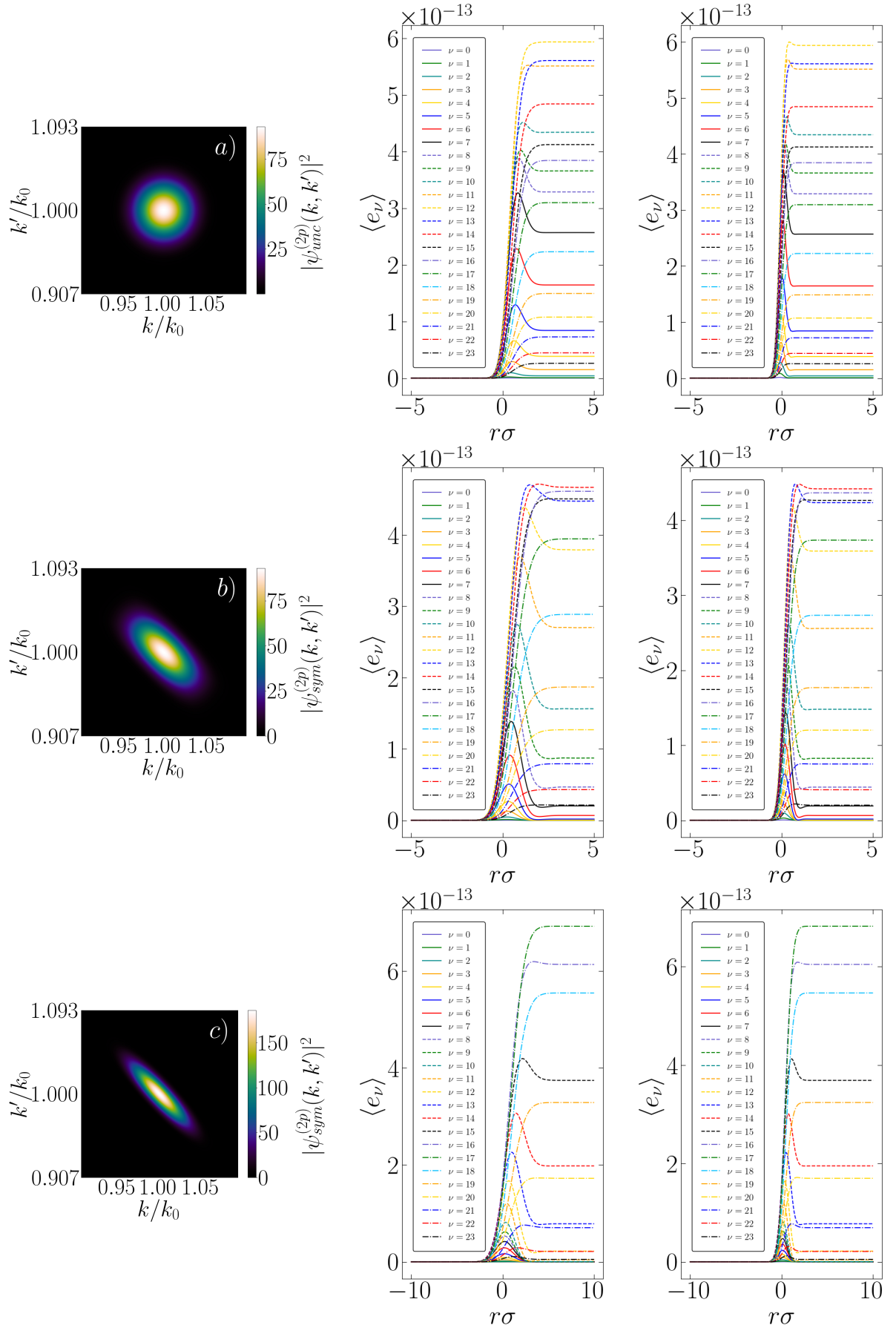


FIG. 4. Population probability of the first 23 excited levels for: a) Uncorrelated photons; b)  $\sigma_s = \sigma$ ; and c)  $\sigma_s = 0.5\sigma$ . In the first column we depict the corresponding JSA. The second column corresponds to the populations calculated numerically. The third column corresponds to the populations calculated by PT.

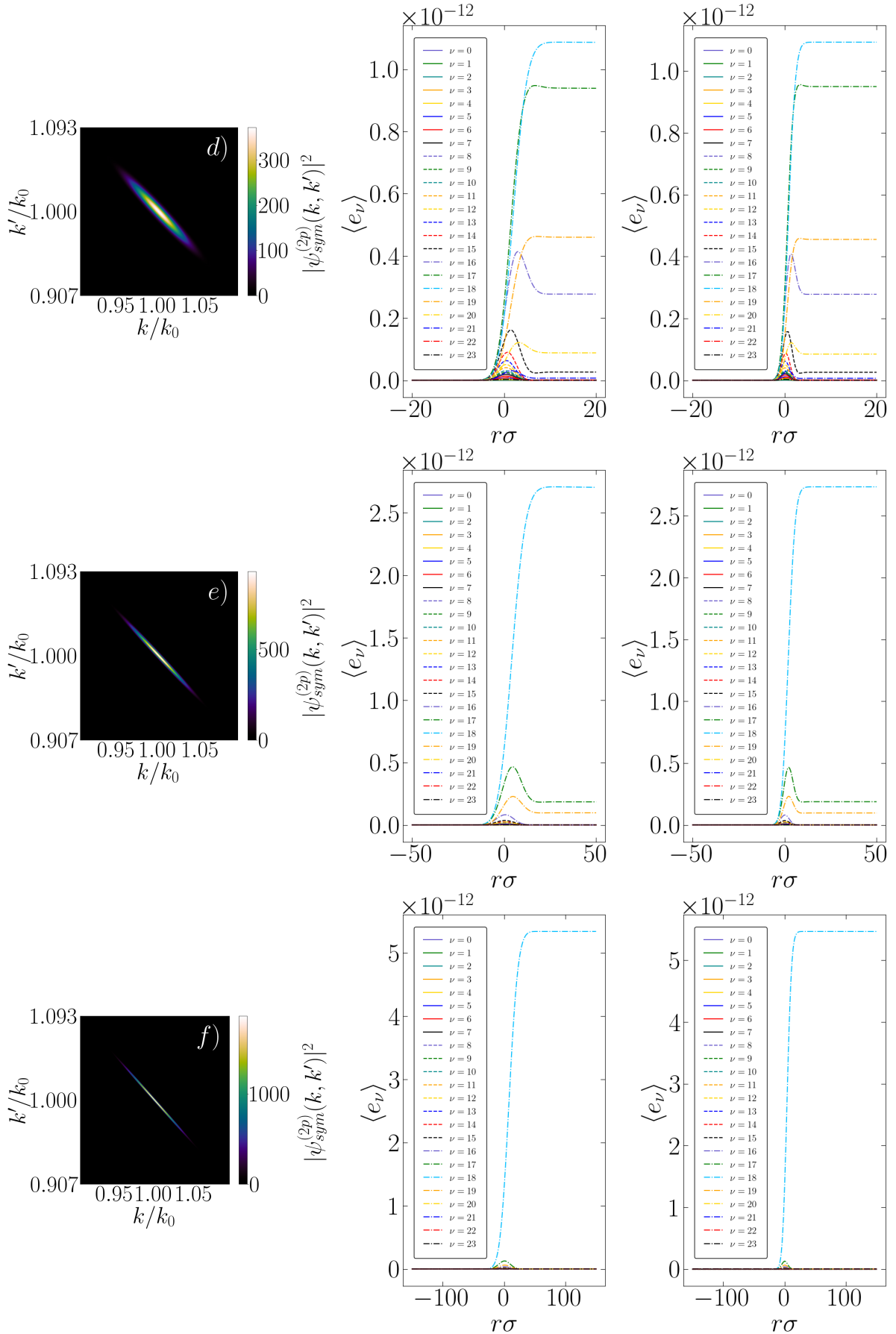


FIG. 5. Continued from Fig. 4. Population probability of the first 23 excited levels for: d)  $\sigma_s = 0.25\sigma$ ; e)  $\sigma_s = 0.1\sigma$ ; and f)  $\sigma_s = 0.05\sigma$ . In the first column we depict the corresponding JSA. The second column corresponds to the populations calculated numerically. The third column corresponds to the populations calculated by PT.

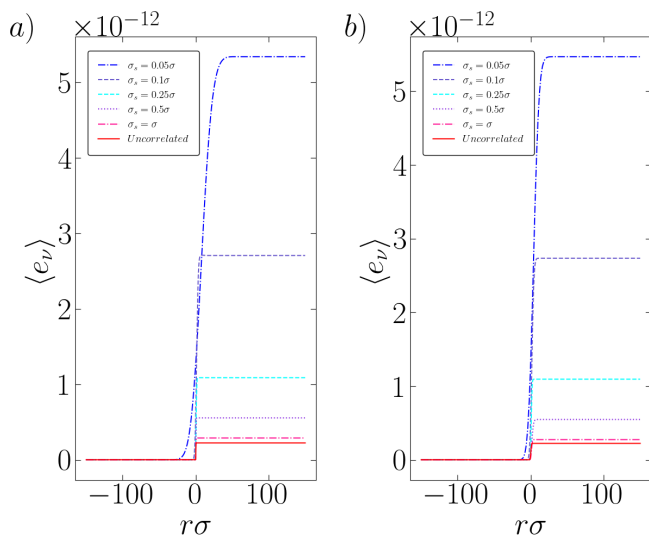


FIG. 6. Evolution of the population of targeted excited sub-level with respect to the correlation degree. a) Populations calculated numerically; b) Populations calculated by PT.

Finally, we remark that the use of our expression drastically reduces the computational effort required by numerical methods. Taking advantage of this, we analyze the selectivity dynamics for different resonance scenarios. That is, we change the central frequency of the entangled photons to be resonant with the first 45 vibrational excited levels, and evaluate the increase in the targeted population to study the dependence of the selectivity on the energy of the chosen level. Fig. 7 depicts this situation.

In Fig. 7 we evaluate the selectivity  $\xi$  defined as

$$\xi = \frac{\langle e_{\nu=\text{Targeted level}} \rangle}{\sum_{\nu} \langle e_{\nu} \rangle}. \quad (59)$$

We can observe a Poisson-distribution-like behavior for the low degree correlations, exhibiting a maximum at  $\alpha = 7$ . This shape is similar of the distribution of the Franck-Condon factors  $F_{\mu}$ . We attribute these fluctuations to numerical errors in the processing of the series for different  $k_0$  and  $\sigma_s$ . For high degree of entanglement, we do not have more this behavior, but we have that, particularly for  $\sigma_s = 0.1\sigma$  the enhancement is reduced for high-energy vibrational levels. For  $\sigma_s = 0.05\sigma$  we obtained the total selection of the targeted levels for all  $\alpha$ . Thus, for this molecular system, if we want to obtain a rapid enhancement of the population as the degree correlation increases, we must concentrate the efforts in obtaining entangled photons with central frequency near to the energy values corresponding to the excited vibrational levels  $5 < \alpha < 10$ . In other words, when we have entangled photons with a high degree of correlation between them, the targeted level will be highly selected, neglecting the vibrational energy. Otherwise, if we experimentally have intermediate entanglement degrees, we can take advantage of the vibrational structure of the molecule to obtain high selectivity with non-high entangled photon pairs.

To understand the influence of the vibrational structure on the behavior observed in Fig. 7, we study the behavior of the

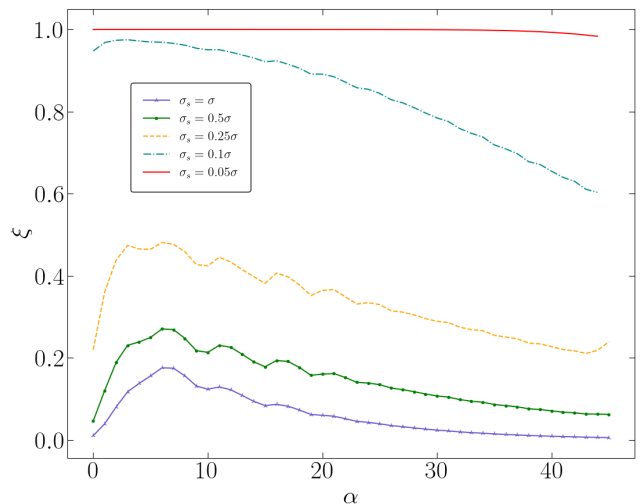


FIG. 7. Selectivity for each energy level in resonance with the central frequency of the photon field.

matrix elements of Eq. (58) for different resonance scenarios. In Fig. 8 we show the case where the central energy of the entangled photons is resonant with the excited vibrational level  $\alpha = 7$  (first column),  $\alpha = 18$  (second column), and  $\alpha = 36$  (third column). This corresponds to values of  $2k_0 \approx 3.8831$  eV,  $2k_0 \approx 4.0024$  eV, and  $2k_0 \approx 4.1614$  eV, respectively. The first row corresponds to the uncorrelated case, i.e.,  $\Theta_{\alpha\nu}^{(u)}$ . The second and third row are the correlated case with  $\sigma_s = 0.5\sigma$ , and  $\sigma_s = 0.1\sigma$ , respectively. We can observe that for  $\alpha = 7$ , the Gaussian functions are allowing the participation of more Franck-Condon factors product  $F_{\nu}F_{\nu\alpha}$ , than in the case of  $\alpha = 18$ , and  $\alpha = 36$ . For  $\alpha = 36$  this participation is substantially reduced even in the uncorrelated case, where we can evidence that only a fraction of the upper branch of the Franck-Condon parabolas is contributing to the transition. Notice that for  $\sigma_s = 0.1\sigma$  (high correlation degree), there is more dispersion for high energy vibrational levels, than observed for low levels. Thus, low energy vibrational levels are more reliable to perform tasks which require rapid enhancement of selectivity.

This analysis shows that the transition matrix, Eq. (58), could help to construct an optimal experimental set up to exploit vibrational selectivity due to entangled photons.

## V. SUMMARY AND OUTLOOK

The discrepancies between the experimental results and theoretical simulations of the ETPA remain an active area of research. Most theoretical works use second-order PT within simplified models and approximations (or fourth-order perturbation in the density matrix formalism) [24, 34, 35, 51, 54, 56, 62]. Although these theoretical works have provided qualitative and phenomenological insights into ETPA processes, their numerical predictions often deviate significantly from experimental measurements. A question then arises regard-

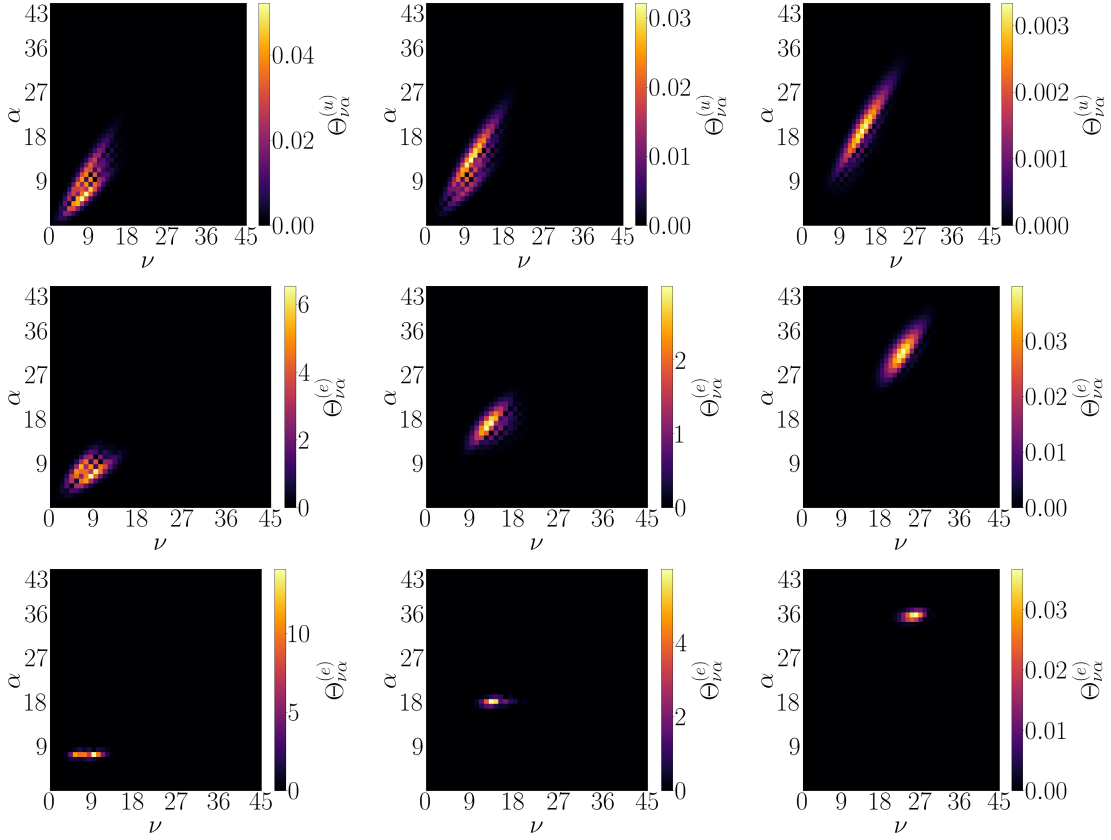


FIG. 8. Behaviour of (58) when the central energy of the entangled photons is resonant with the excited vibrational level  $\alpha = 7$ ,  $2k_0 \approx 3.8831$  eV, (first column),  $\alpha = 18$  (second column),  $2k_0 \approx 4.0024$  eV, and  $\alpha = 36$ ,  $2k_0 \approx 4.1614$  eV, (third column). The first row corresponds to the uncorrelated case, i.e.  $\Theta_{\nu\alpha}^{(u)}$ . The second and third row are the correlated case with  $\sigma_s = 0.5\sigma$ , and  $\sigma_s = 0.1\sigma$ , respectively.

ing the validity of the approximations used in these studies. In this paper, we have examined this question by relaxing typical approximations done when deploying second-order order PT and investigate the dynamics of vibronic populations of diatomic system excited by ultrabroadband frequency-entangled photons—a model system that has previously been studied via exact numerical solutions of the quantum dynamics of the system [64]. We show that our efficient analytical framework reproduces the results obtained via numerical solution of the complete Schrödinger equation, while providing additional physical insight.

Specifically, using second-order PT that keeps: i) the temporal integrals in a finite time ( $-t_0 \leq t < \infty$ ); ii) the functions to be integrated on the frequency domain without any asymptotic approximations regarding resonance or far from resonance; and iii) the rapid convergent series representation of the transition amplitudes, we obtained the same excited state dynamics as that predicted by solving a system of more than  $25 \times 10^6$  coupled differential equations [57]. These steps allowed us to arrive at analytical expressions that capture the light-matter correlations that affect the TPA processes.

The structure of our analytical expressions in Eq. (41), and Eq. (48) provides an understanding of the nature of the TPA processes depending on the correlations in the light source. First, Eq. (41) shows that CTPA can be seen as a multi-

plicative single-photon processes of transitions from ground states to intermediate states and from intermediate to excited states. In contrast, ETPA transition (48) becomes a weighted average of two differentiated one-photon transitions, modulated by a Gaussian envelope that captures the resonance or off-resonance conditions and the degree of two-photon correlation. These results allow us to understand the key physical differences in vibronic excitation with uncorrelated and quantum-correlated photons. Furthermore, we have extended the analysis presented in Ref. [64] investigating the population dynamics and vibronic selectivity for intermediate photon correlations degrees. We showed that a high correlation degree is not always essential for achieving a substantial enhancement of the targeted vibrational state.

Our analytical expression for the population of the targeted vibrational state reveals a factor that explains (and potentially quantifies) the quantum enhancement of the population selectivity. Combined with the product of the Franck-Condon factors  $F_\nu F_{\nu\alpha}$ , which we refer to as the transition matrix (defined in Eq. 58), this factor provides insight into the maximum achievable population with each correlation degree. Additionally, this matrix reveals how the correlation degree of the entangled photons shape the participation of the Franck-Condon factors in the transitions. Therefore, the structure defined in Eq. (58) may assist in designing optimal experimental setups

to leverage the vibrational selectivity through entangled photons.

We also explored different resonance scenarios to understand the selectivity properties. Taking advantage of the low computational effort required by our approach, we studied simulations of the population for different targeted levels as a function of the number of entangled modes in the biphoton state, and the molecular structure. We show that it is possible to obtain high selectivity with a low degree of correlation, if the targeted vibrational level has associated high values of the Franck-Condon factors transitions. In our particular case, we can expect high selectivity from a reduced entanglement degree if the targeted level is between levels  $\alpha = 7$  and  $\alpha = 10$ . We observed that for low photon correlation degrees, the functional form of the selectivity is related with the Franck-Condon factors  $F_\mu$  structure.

Our results are consistent with those in Ref. [61]. Accounting for a non-simplified molecular electronic structure has yielded insights into experimentally observed phenomena, such as a red-shift of peaks between CTPA and ETPA. The analytical framework we derived supports assumptions that suggest that the quantum correlations of molecular states interact with the quantum correlations of entangled photons. These interactions constitute a foundational basis for understanding this phenomenon. Regarding this aspect, we obtained a structure that describes the involvement of molecular levels correlations (encoded in the Franck-Condon factors) and their contributions in ETPA dynamics.

We have examined ultrabroad-band frequency entangled photons which avoid usual labeling of the entangled photons generated by SPDC as idler and signal photons. An extension of this work is to implement other kinds of JSA's containing information on pump time, entanglement time and entanglement area, which are parameters that can be accessed and modified in experimental setups.

It would also be interesting to extend the framework developed here to investigate the relevance of the vibrational structures for ETPA of widely investigated molecular systems such as ZnTPP and rhodamine B (RhB), but also for the quantum-light activation of relevant photosensitive proteins (e.g., light-oxygen-voltage (LOV) domains [86]) that are engineered as fluorescent labels or as optogenetic tools [87, 88]. Investigating the activation of such photosensors with quantum states of light may provide insight into the possible advantages of ETPA for targeted control in biology.

In our work, the system considered has a vibrational structure that is modeled by a Morse potential with the vibrational transitions described within the Franck-Condon approximation. However, a variety of molecules of chemical and biological significance have a vibrational structure that includes Herzberg-Teller couplings. A possible interesting extension of our work is to investigate the effect of Herzberg-Teller coupling in ETPA [89–91]. Finally, our framework can be adapted to investigate the advantages of plasmonic structures as a promising avenue to improve signal acquisition in ETPA measurements [92–97]. These topics are the subject of our future studies.

## ACKNOWLEDGMENTS

We would like to thank Chawntell Kulkarni, Sougato Bose, Andrew Fisher, Robert Thew, Karolina Słowik, and Anita Dabrowska for their helpful discussions. We gratefully acknowledge the funding from the Engineering and Physical Sciences Research Council (EPSRC) (Grants No. EP/R513143/1 and No. EP/T517793/1) and the Gordon and Betty Moore Foundation (Grant 8820).

## Appendix A: Discretized Schrodinger equations

In this section, we derive the discretized form of the Schrödinger equations and matrix definitions for subsequent computational implementation. To solve the equations (54), (55), and (56), we discretize the photon fields by converting from  $\int dk$  to  $\sum_k \delta k$ , and  $\hat{a}(k)$  to  $\hat{a}_k$ . The discretized equations have the following form

$$\begin{aligned} \frac{d}{dt}\psi_{kk'}^{(2p)}(t) = & -i(k+k')\psi_{kk'}^{(2p)}(t) \\ & -i\sum_v\sqrt{\frac{\gamma F_v}{2\pi}}\left[\psi_{kv}^{(1pm)}(t)+\psi_{k'v}^{(1pm)}(t)\right] \end{aligned} \quad (\text{A1})$$

$$\begin{aligned} \frac{d}{dt}\psi_{kv}^{(1pm)}(t) = & -i(k+\omega_{m_v})\psi_{kv}^{(1pm)}(t) \\ & -i\sqrt{\frac{2\gamma F_v}{\pi}}\sum_{k'}\delta k\psi_{kk'}^{(2p)}(t) \\ & -i\sum_{v'}\sqrt{\frac{\gamma F_{vv'}}{\pi}}\psi_{v'}^{(e)}(t) \end{aligned} \quad (\text{A2})$$

$$\frac{d}{dt}\psi_{v'}^{(e)}(t) = -i\omega_{e_v}\psi_{v'}^{(e)}(t) - i\sum_{vv'}\sqrt{\frac{\gamma F_{vv'}}{\pi}}\sum_k\delta k\psi_{kv}^{(1pm)}(t) \quad (\text{A3})$$

Defining the following matrices which are containing the functions for each state

$$\psi^{(2p)} = \begin{pmatrix} \psi_{k_0k_0}^{(2p)} & \psi_{k_0k_1}^{(2p)} & \cdots & \psi_{k_0k_M}^{(2p)} \\ \psi_{k_1k_0}^{(2p)} & \psi_{k_1k_1}^{(2p)} & \cdots & \psi_{k_1k_M}^{(2p)} \\ \vdots & \vdots & \cdots & \vdots \\ \psi_{k_Mk_0}^{(2p)} & \psi_{k_Mk_1}^{(2p)} & \cdots & \psi_{k_Mk_M}^{(2p)} \end{pmatrix} \quad (\text{A4})$$

$$\psi^{(1pm)} = \begin{pmatrix} \psi_{k_0,0}^{(1pm)} & \psi_{k_0,1}^{(1pm)} & \cdots & \psi_{k_0,N}^{(1pm)} \\ \psi_{k_1,0}^{(1pm)} & \psi_{k_1,1}^{(1pm)} & \cdots & \psi_{k_1,N}^{(1pm)} \\ \vdots & \vdots & \cdots & \vdots \\ \psi_{k_M,0}^{(1pm)} & \psi_{k_M,1}^{(1pm)} & \cdots & \psi_{k_M,N}^{(1pm)} \end{pmatrix} \quad (\text{A5})$$

$$\psi^e = \begin{pmatrix} \psi_0^e \\ \psi_1^e \\ \vdots \\ \psi_N^e \end{pmatrix} \quad (\text{A6})$$

$$\gamma = \begin{pmatrix} \gamma_0 \\ \gamma_1 \\ \vdots \\ \gamma_N \end{pmatrix} \quad (\text{A7})$$

$$\gamma^{(gm)} = \begin{pmatrix} \gamma_0 & \gamma_1 & \cdots & \gamma_N \\ \gamma_0 & \gamma_1 & \cdots & \gamma_N \\ \vdots & \vdots & \cdots & \vdots \\ \gamma_0 & \gamma_1 & \cdots & \gamma_N \end{pmatrix} \quad (\text{A8})$$

$$\gamma^{(me)} = \begin{pmatrix} \gamma_{00} & \gamma_{01} & \cdots & \gamma_{0N} \\ \gamma_{10} & \gamma_{11} & \cdots & \gamma_{1N} \\ \vdots & \vdots & \cdots & \vdots \\ \gamma_{N0} & \gamma_{N1} & \cdots & \gamma_{NN} \end{pmatrix} \quad (\text{A9})$$

the discretized form of the set of differential equations is given by

$$\begin{aligned} \frac{d}{dt} \psi_{k_\alpha k_\beta}^{(2p)} = & -i(k_\alpha + k_\beta) \psi_{k_\alpha k_\beta}^{(2p)} \\ & -i(\psi^{(1pm)} \gamma)_\alpha - i(\psi^{(1pm)} \gamma)_\beta \end{aligned} \quad (\text{A10})$$

$$\begin{aligned} \frac{d}{dt} \psi_{k_\alpha j}^{(1pm)} = & -i(k_\alpha + \omega_{m_j}) \psi_{k_\alpha j}^{(1pm)} \\ & -i(\psi^{(2p)} \gamma^{(gm)})_{\alpha j} - i(\gamma^{(me)} \psi^e)_j \end{aligned} \quad (\text{A11})$$

$$\frac{d}{dt} \psi_j^e = -i\omega_{e_j} \psi_j^e - i \sum_{n=0}^N (\psi^{(1pm)} \gamma^{(me)})_{nj}. \quad (\text{A12})$$

The matrix notation has allowed us to significantly improve the computational speed of solving the full set of differential equations. This structure facilitates the use of optimized NumPy functions, enabling faster computations and making it easier to implement various pre-installed solver tools.

## Appendix B: Dynamics of $\langle m_\nu \rangle$

As a matter of completeness, we include the population dynamics of the first 23 intermediate states  $\langle m_\nu \rangle$  for uncorrelated photons, Fig. 9, and an intermediate entanglement degree, Fig. 10. Here, as is shown in the work of H. Oka, we can observe the natural dynamics of a TSE process where the intermediate states are actually excited. From the depicted results, we find that the resultant populations do not depend on the degree of quantum correlation of the photons, and confirms the tendency showed in the aforementioned work.

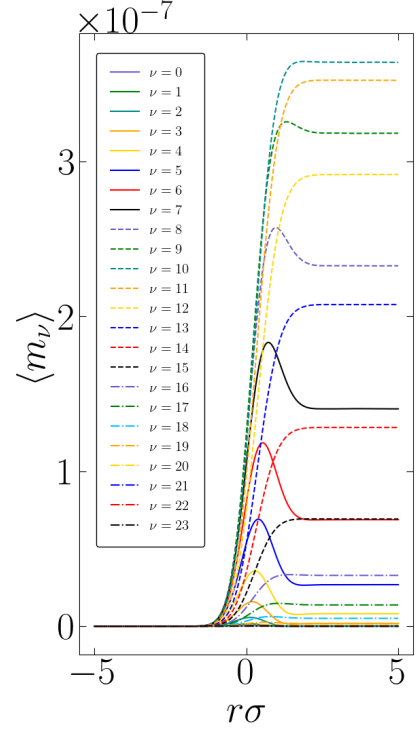


FIG. 9. Dynamics of  $\langle m_\nu \rangle$  as a function of  $r\sigma$  within the JSA (7).

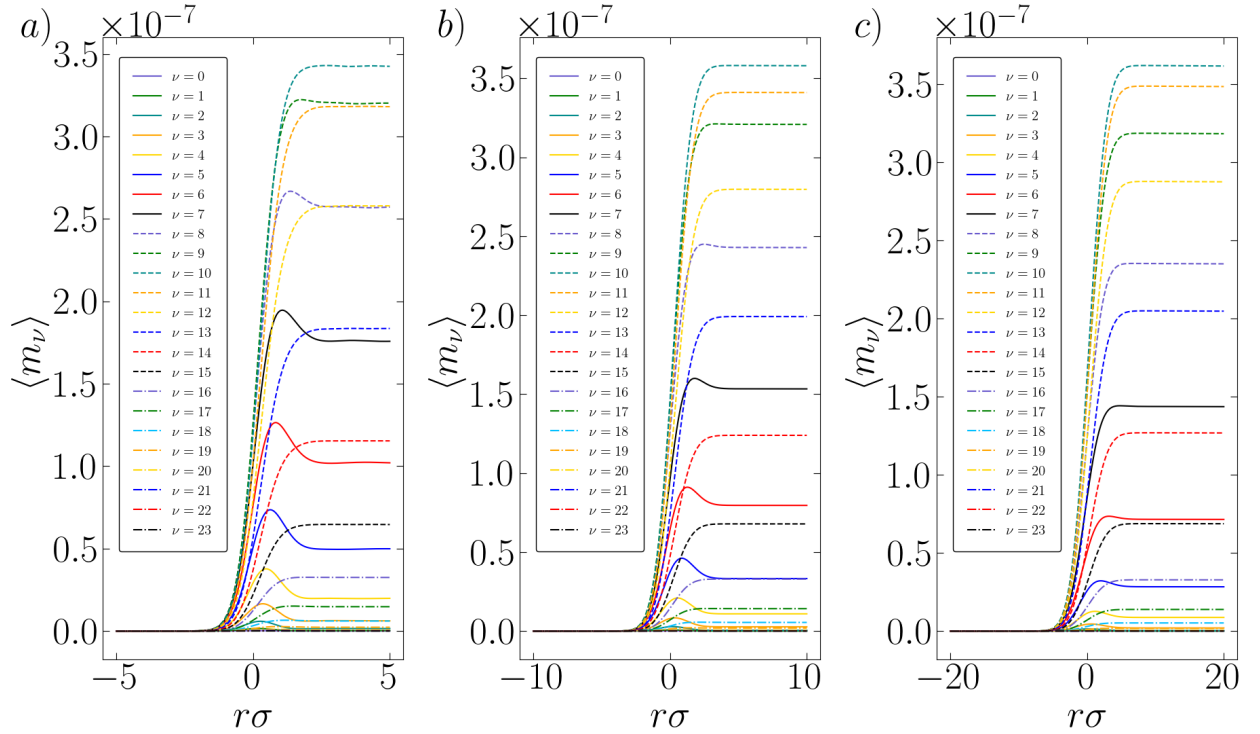


FIG. 10. Dynamics of  $\langle m_\nu \rangle$  as a function of  $r\sigma$  within the JSA (9) for: a)  $\sigma_s = \sigma$ ; b)  $\sigma_s = 0.5\sigma$ ; and c)  $\sigma_s = 0.25\sigma$ . For correlated photons, the absorption is slower and resonant, while in the uncorrelated case, the oscillation of population, commonly found in near-resonant absorption, is arising

### Appendix C: Explicit form of $I_{\nu\alpha}^{(u)}(t, t_0)$ , $I_{\nu\alpha}^{(en,1)}(t, t_0)$ and $I_{\nu\alpha}^{(en,2)}(t, t_0)$

In this appendix, we present the explicit forms of the functions inside the representation series of the transition probabilities. Let us start with Eq. (44) for the case of uncorrelated photons. Function  $f_{n,l}^{(u,1)}(t, t_0)$  is defined as follows:

$$f_{n,l}^{(u,1)}(t, t_0) = \frac{(2t\sigma^2 - i(k_0 - \omega_{m_\nu}))^{2l}}{(2it\sigma^2 + k_0 - \Omega_{\alpha\nu})^{-2n}} \Delta F_1, \quad (C1)$$

being

$$\begin{aligned} \Delta F_1 = & F_1 \left( 2; -2l, -2n; 3; \frac{2it\sigma^2}{-2it\sigma^2 - k_0 + \omega_{m_\nu}}, \frac{2it\sigma^2}{2it\sigma^2 + k_0 - \Omega_{\alpha\nu}} \right) \\ & - F_1 \left( 2; -2l, -2n; 3; \frac{2t_0\sigma^2}{2t\sigma^2 - i(k_0 - \omega_{m_\nu})}, \frac{2it_0\sigma^2}{2it\sigma^2 + k_0 - \Omega_{\alpha\nu}} \right), \end{aligned} \quad (C2)$$

where  $F_1(a; b_1, b_2; c; x, y)$  is the Appell hypergeometric function of two variables.

On the other hand, the function  $f_{n,l}^{(u,2)}(t, t_0)$  is defined as follows:

$$\begin{aligned} f_{n,l}^{(u,2)}(t, t_0) = & \frac{(4t\sigma^2 - i(k_0 - \omega_{m_\nu}))^{2l+1}}{(4it\sigma^2 - k_0 + \Omega_{\alpha\nu})^{-2n-1}} {}_2F_1 \left( 1, 2(n+l+1); 2(n+1); \frac{-4it\sigma^2 - k_0 + \Omega_{\alpha\nu}}{\omega_{e_\alpha} - 2\omega_{m_\nu}} \right) \\ & - \frac{(2(t-t_0)\sigma^2 - i(k_0 - \omega_{m_\nu}))^{2l+1}}{(2i(t-t_0)\sigma^2 + k_0 - \Omega_{\alpha\nu})^{-2n-1}} {}_2F_1 \left( 1, 2(n+l+1); 2(n+1); \frac{-2i(t-t_0)\sigma^2 - k_0 + \Omega_{\alpha\nu}}{\omega_{e_\alpha} - 2\omega_{m_\nu}} \right), \end{aligned} \quad (C3)$$

where  ${}_2F_1(a, b, c; z)$  is the hypergeometric function.

For the entangled photons case, the term  $I_{\nu\alpha}^{(en,1)}(t, t_0)$  in (50) is defined as

$$I_{\nu\alpha}^{(en,1)}(t, t_0) = \frac{1}{2\pi} \sum_{n,l=0}^{\infty} \frac{4^{-n-l}\sigma^{-2l-3}\sigma_s^{-2n+1}}{n!l!(2l+1)(2l+3)} \left[ \frac{f_{n,l}^{(e,1)}(t) + f_{n,l}^{(e,2)}(t, t_0)}{4it\sigma^2\sigma_s^2 - \sigma^2(2k_0 - \omega_{e_\alpha}) + \sigma_s^2(k_0 - \omega_{m_\nu})} \right], \quad (C4)$$



being

$$f_{n,l}^{(e,1)}(t) = \frac{(-1)^l (k_0 - \omega_{m_v})^{2l+3}}{(4t\sigma_s^2 + i(2k_0 - \omega_{e_a}))^{-2n-1}} {}_2F_1 \left( 1, 2(n+l+2); 2(l+2); \frac{\sigma_s^2(k_0 - \omega_{m_v})}{4it\sigma^2\sigma_s^2 - \sigma^2(2k_0 - \omega_{e_a}) + \sigma_s^2(k_0 - \omega_{m_v})} \right), \quad (C5)$$

and

$$f_{n,l}^{(e,2)}(t, t_0) = \frac{i(2\sigma^2(t+t_0) - i(k_0 - \omega_{m_v}))^{2l+3}}{(2\sigma_s^2(t-t_0) + i(2k_0 - \omega_{e_a}))^{-2n-1}} {}_2F_1 \left( 1, 2(n+l+2); 2(l+2); \frac{i\sigma_s^2(2\sigma^2(t+t_0) - i(k_0 - \omega_{m_v}))}{4it\sigma^2\sigma_s^2 - \sigma^2(2k_0 - \omega_{e_a}) + \sigma_s^2(k_0 - \omega_{m_v})} \right). \quad (C6)$$

Now, the term  $I_{va}^{(en,2)}(t, t_0)$  in (51) is defined as

$$I_{va}^{(en,2)}(t, t_0) = \frac{4}{\pi \sqrt{\sigma^2 + \sigma_s^2}} \left\{ \frac{1}{\sigma^2} \sum_{n,l=0}^{\infty} c_{nl} f_{n,l}^{(e,3)}(t, t_0) + \frac{i}{\sigma_s^2} \sum_{n,l'=0}^{\infty} c_{n,l'} f_{n,l'}^{(e,4)}(t, t_0) \right\}, \quad (C7)$$

being

$$c_{nl} = \frac{2^{-2(n+l)-3} \Gamma(2n+1) (\sigma\sigma_s)^{-2n+1}}{n!!(2l+1)(\sigma^2 + \sigma_s^2)^{n+l+2}} \quad (C8)$$

$$\begin{aligned} f_{n,l}^{(e,3)}(t, t_0) &= \frac{(2i\sigma^2(t+t_0) + 4it\sigma_s^2 + k_0 - \omega_{m_v})^{2l+3}}{(-2i\sigma^2\sigma_s^2(t-t_0) - \sigma^2(2k_0 - \omega_{e_a}) - \sigma_s^2(k_0 - \Omega_{av}))^{-2n-1}} \\ &\times {}_2F_1^R \left( 1, 2(n+l+2); 2(n+1); \frac{2i\sigma^2\sigma_s^2(t-t_0) + \sigma^2(2k_0 - \omega_{e_a}) + \sigma_s^2(k_0 - \Omega_{av})}{(\sigma^2 + \sigma_s^2)(4it\sigma_s^2 + 2k_0 + \omega_{e_a})} \right) \\ &+ \frac{(4it\sigma_s^2 + k_0 - \omega_{m_v})^{2l+3}}{(4it\sigma^2\sigma_s^2(t-t_0) + \sigma^2(2k_0 - \omega_{e_a}) + \sigma_s^2(k_0 - \Omega_{av}))^{-2n-1}} \\ &\times {}_2F_1^R \left( 1, 2(n+l+2); 2(n+1); \frac{4it\sigma_s^2 + \sigma^2(2k_0 - \omega_{e_a}) + \sigma_s^2(k_0 - \Omega_{av})}{(\sigma^2 + \sigma_s^2)(4it\sigma_s^2 + 2k_0 + \omega_{e_a})} \right), \end{aligned} \quad (C9)$$

and

$$\begin{aligned} f_{n,l'}^{(e,4)}(t, t_0) &= \frac{(-1)^{1-l'} (-2\sigma_s^2(t-t_0) + i(k_0 - \omega_{m_v}))^{2l'+3}}{(-2i\sigma^2\sigma_s^2(t-t_0) - \sigma^2(2k_0 - \omega_{e_a}) - \sigma_s^2(k_0 - \Omega_{av}))^{-2n-1}} \\ &\times {}_2F_1^R \left( 1, 2(n+l'+2); 2(n+1); \frac{2i\sigma^2\sigma_s^2(t-t_0) + \sigma^2(2k_0 - \omega_{e_a}) + \sigma_s^2(k_0 - \Omega_{av})}{(\sigma^2 + \sigma_s^2)(k_0 - \Omega_{av})} \right) \\ &+ \frac{i(4it\sigma_s^2 + k_0 - \omega_{m_v})^{2l'+3}}{(4it\sigma^2\sigma_s^2(t-t_0) + \sigma^2(2k_0 - \omega_{e_a}) + \sigma_s^2(k_0 - \Omega_{av}))^{-2n-1}} \\ &\times {}_2F_1^R \left( 1, 2(n+l'+2); 2(n+1); \frac{4it\sigma_s^2 + \sigma^2(2k_0 - \omega_{e_a}) + \sigma_s^2(k_0 - \Omega_{av})}{(\sigma^2 + \sigma_s^2)(k_0 - \Omega_{av})} \right). \end{aligned} \quad (C10)$$

Where  ${}_2F_1^R(a, b; c; z)$  is the regularized hypergeometric function given by  ${}_2F_1^R(a, b; c; z) = {}_2F_1(a, b; c; z)/\Gamma(c)$ , being  $\Gamma(z)$  the Gamma function. These series representations, composed of error functions and hypergeometric functions, show the intricate relationships between the photons quantum correlations and the vibrational structure.

- 
- [1] S. Pirandola, J. Eisert, C. Weedbrook, A. Furusawa, and S. L. Braunstein, Advances in quantum teleportation, *Nature photonics* **9**, 641 (2015).  
 [2] X.-M. Hu, Y. Guo, B.-H. Liu, C.-F. Li, and G.-C. Guo, Progress in quantum teleportation, *Nature Reviews Physics* **5**, 339 (2023).

- [3] R. Ursin, F. Tiefenbacher, T. Schmitt-Manderbach, H. Weier, T. Scheidl, M. Lindenthal, B. Blauensteiner, T. Jennewein, J. Perdigues, P. Trojek, *et al.*, Entanglement-based quantum communication over 144 km, *Nature physics* **3**, 481 (2007).  
 [4] N. Zou, Quantum entanglement and its application in quantum communication, in *Journal of Physics: Conference Series*, Vol.

- 1827 (IOP Publishing, 2021) p. 012120.
- [5] K. Azuma, S. E. Economou, D. Elkouss, P. Hilaire, L. Jiang, H.-K. Lo, and I. Tzitrin, Quantum repeaters: From quantum networks to the quantum internet, *Reviews of Modern Physics* **95**, 045006 (2023).
  - [6] S. Pirandola, U. L. Andersen, L. Banchi, M. Berta, D. Bunandar, R. Colbeck, D. Englund, T. Gehring, C. Lupo, C. Ottaviani, *et al.*, Advances in quantum cryptography, *Advances in optics and photonics* **12**, 1012 (2020).
  - [7] L. Pezzè, A. Smerzi, M. K. Oberthaler, R. Schmied, and P. Treutlein, Quantum metrology with nonclassical states of atomic ensembles, *Rev. Mod. Phys.* **90**, 035005 (2018).
  - [8] E. Polino, M. Valeri, N. Spagnolo, and F. Sciarrino, Photonic quantum metrology, *AVS Quantum Science* **2** (2020).
  - [9] M. A. Taylor and W. P. Bowen, Quantum metrology and its application in biology, *Physics Reports* **615**, 1 (2016), quantum metrology and its application in biology.
  - [10] G. B. Lemos, V. Borish, G. D. Cole, S. Ramelow, R. Lapkiewicz, and A. Zeilinger, Quantum imaging with undetected photons, *Nature* **512**, 409 (2014).
  - [11] M. Lahiri, R. Lapkiewicz, G. B. Lemos, and A. Zeilinger, Theory of quantum imaging with undetected photons, *Phys. Rev. A* **92**, 013832 (2015).
  - [12] A. Vega, E. A. Santos, J. Fuenzalida, M. Gilaberte Basset, T. Pertsch, M. Gräfe, S. Saravi, and F. Setzpfandt, Fundamental resolution limit of quantum imaging with undetected photons, *Phys. Rev. Res.* **4**, 033252 (2022).
  - [13] G. Barreto Lemos, M. Lahiri, S. Ramelow, R. Lapkiewicz, and W. N. Plick, Quantum imaging and metrology with undetected photons: tutorial, *Journal of the Optical Society of America B* **39**, 2200 (2022).
  - [14] C. L. Degen, F. Reinhard, and P. Cappellaro, Quantum sensing, *Rev. Mod. Phys.* **89**, 035002 (2017).
  - [15] S. Pirandola, B. R. Bardhan, T. Gehring, C. Weedbrook, and S. Lloyd, Advances in photonic quantum sensing, *Nature Photonics* **12**, 724 (2018).
  - [16] F. Schlawin and S. Mukamel, Two-photon spectroscopy of excitons with entangled photons, *The Journal of chemical physics* **139**, <https://doi.org/10.1063/1.4848739> (2013).
  - [17] M. Richter and S. Mukamel, Ultrafast double-quantum-coherence spectroscopy of excitons with entangled photons, *Phys. Rev. A* **82**, 013820 (2010).
  - [18] Y. Fujihashi, K. Miwa, M. Higashi, and A. Ishizaki, Probing exciton dynamics with spectral selectivity through the use of quantum entangled photons. *The Journal of Chemical Physics* **159**, <https://doi.org/10.1063/5.0169768> (2023).
  - [19] A. M. Zheltikov and M. O. Scully, Photon entanglement for life-science imaging: rethinking the limits of the possible, *Physics-Usp ekhi* **63**, 698 (2020).
  - [20] W. Zong, R. Wu, S. Chen, J. Wu, H. Wang, Z. Zhao, G. Chen, R. Tu, D. Wu, Y. Hu, *et al.*, Miniature two-photon microscopy for enlarged field-of-view, multi-plane and long-term brain imaging, *Nature methods* **18**, 46 (2021).
  - [21] A. R. Guzman, M. R. Harpham, O. Süzer, M. M. Haley, and T. G. Goodson III, Spatial control of entangled two-photon absorption with organic chromophores, *Journal of the American Chemical Society* **132**, 7840 (2010).
  - [22] L. Upton, M. Harpham, O. Süzer, M. Richter, S. Mukamel, and T. Goodson III, Optically excited entangled states in organic molecules illuminate the dark, *The Journal of Physical Chemistry Letters* **4**, 2046 (2013).
  - [23] O. Varnavski, C. Gunthardt, A. Rehman, G. D. Luker, and T. Goodson III, Quantum light-enhanced two-photon imaging of breast cancer cells, *The Journal of Physical Chemistry Letters* **13**, 2772 (2022).
  - [24] K. E. Dorfman, F. Schlawin, and S. Mukamel, Nonlinear optical signals and spectroscopy with quantum light, *Rev. Mod. Phys.* **88**, 045008 (2016).
  - [25] O. Varnavski, B. Pinsky, and T. Goodson III, Entangled photon excited fluorescence in organic materials: an ultrafast coincidence detector, *The journal of physical chemistry letters* **8**, 388 (2017).
  - [26] G. Kang, K. Nasiri Avanaki, M. A. Mosquera, R. K. Burdick, J. P. Villabona-Monsalve, T. Goodson III, and G. C. Schatz, Efficient modeling of organic chromophores for entangled two-photon absorption, *Journal of the American Chemical Society* **142**, 10446 (2020).
  - [27] R. K. Burdick, O. Varnavski, A. Molina, L. Upton, P. Zimmerman, and T. Goodson III, Predicting and controlling entangled two-photon absorption in diatomic molecules, *The Journal of Physical Chemistry A* **122**, 8198 (2018).
  - [28] A. Eshun, O. Varnavski, J. P. Villabona-Monsalve, R. K. Burdick, and T. Goodson III, Entangled photon spectroscopy, *Accounts of Chemical Research* **55**, 991 (2022).
  - [29] S. Szoke, H. Liu, B. P. Hickam, M. He, and S. K. Cushing, Entangled light-matter interactions and spectroscopy, *Journal of Materials Chemistry C* **8**, 10732 (2020).
  - [30] F. Schlawin, K. E. Dorfman, and S. Mukamel, Entangled two-photon absorption spectroscopy, *Accounts of chemical research* **51**, 2207 (2018).
  - [31] S. Mukamel, M. Freyberger, W. Schleich, M. Bellini, A. Zavatta, G. Leuchs, C. Silberhorn, R. W. Boyd, L. L. Sánchez-Soto, A. Stefanov, M. Barbieri, A. Paterova, L. Krivitsky, S. Shwartz, K. Tamasaku, K. Dorfman, F. Schlawin, V. Sandoghdar, M. Raymer, A. Marcus, O. Varnavski, T. Goodson, Z.-Y. Zhou, B.-S. Shi, S. Asban, M. Scully, G. Agarwal, T. Peng, A. V. Sokolov, Z.-D. Zhang, M. S. Zubairy, I. A. Vartanyants, E. del Valle, and F. Laussy, Roadmap on quantum light spectroscopy, *Journal of Physics B: Atomic, Molecular and Optical Physics* **53**, 072002 (2020).
  - [32] B. Gu, D. Keefer, F. Aleotti, A. Nenov, M. Garavelli, and S. Mukamel, Photoisomerization transition state manipulation by entangled two-photon absorption, *Proceedings of the National Academy of Sciences* **118**, e2116868118 (2021).
  - [33] T. Landes, M. Allgaier, S. Merkouche, B. J. Smith, A. H. Marcus, and M. G. Raymer, Experimental feasibility of molecular two-photon absorption with isolated time-frequency-entangled photon pairs, *Phys. Rev. Res.* **3**, 033154 (2021).
  - [34] H.-B. Fei, B. M. Jost, S. Popescu, B. E. A. Saleh, and M. C. Teich, Entanglement-induced two-photon transparency, *Phys. Rev. Lett.* **78**, 1679 (1997).
  - [35] F. Lissandrin, B. E. A. Saleh, A. V. Sergienko, and M. C. Teich, Quantum theory of entangled-photon photoemission, *Phys. Rev. B* **69**, 165317 (2004).
  - [36] O. Varnavski and T. Goodson III, Two-photon fluorescence microscopy at extremely low excitation intensity: The power of quantum correlations, *Journal of the American Chemical Society* **142**, 12966 (2020).
  - [37] J. Javanainen and P. L. Gould, Linear intensity dependence of a two-photon transition rate, *Phys. Rev. A* **41**, 5088 (1990).
  - [38] W. L. Peticolas, Multiphoton spectroscopy, *Annual Review of Physical Chemistry* **18**, 233 (1967).
  - [39] J. P. Villabona-Monsalve, O. Calderón-Losada, M. Nuñez Portela, and A. Valencia, Entangled two photon absorption cross section on the 808 nm region for the common dyes zinc tetraphenylporphyrin and rhodamine b, *The Journal of Physical Chemistry A* **121**, 7869 (2017).
  - [40] A. Eshun, Z. Cai, M. Awies, L. Yu, and T. Goodson III, Inves-

- tigations of thienoacene molecules for classical and entangled two-photon absorption, *The Journal of Physical Chemistry A* **122**, 8167 (2018).
- [41] D. Tabakaev, A. Djorović, L. La Volpe, G. Gaulier, S. Ghosh, L. Bonacina, J.-P. Wolf, H. Zbinden, and R. T. Thew, Spatial properties of entangled two-photon absorption, *Phys. Rev. Lett.* **129**, 183601 (2022).
- [42] D. Tabakaev, M. Montagnese, G. Haack, L. Bonacina, J.-P. Wolf, H. Zbinden, and R. T. Thew, Energy-time-entangled two-photon molecular absorption, *Phys. Rev. A* **103**, 033701 (2021).
- [43] J. P. Villabona-Monsalve, O. Varnavski, B. A. Palfey, and T. Goodson III, Two-photon excitation of flavins and flavoproteins with classical and quantum light, *Journal of the American Chemical Society* **140**, 14562 (2018).
- [44] M. He, B. P. Hickam, N. Harper, and S. K. Cushing, Experimental upper bounds for resonance-enhanced entangled two-photon absorption cross section of indocyanine green, *The Journal of Chemical Physics* **160**, 094305 (2024).
- [45] T. Landes, B. J. Smith, and M. G. Raymer, Limitations in fluorescence-detected entangled two-photon-absorption experiments: Exploring the low- to high-gain squeezing regimes, *Phys. Rev. A* **110**, 033708 (2024).
- [46] B. P. Hickam, M. He, N. Harper, S. Szoke, and S. K. Cushing, Single-photon scattering can account for the discrepancies among entangled two-photon measurement techniques, *The Journal of Physical Chemistry Letters* **13**, 4934 (2022), pMID: 35635002.
- [47] K. M. Parzuchowski, A. Mikhaylov, M. D. Mazurek, R. N. Wilson, D. J. Lum, T. Gerrits, C. H. Camp, M. J. Stevens, and R. Jimenez, Setting bounds on entangled two-photon absorption cross sections in common fluorophores, *Phys. Rev. Appl.* **15**, 044012 (2021).
- [48] B. E. A. Saleh, B. M. Jost, H.-B. Fei, and M. C. Teich, Entangled-photon virtual-state spectroscopy, *Phys. Rev. Lett.* **80**, 3483 (1998).
- [49] J. Peřina, B. E. A. Saleh, and M. C. Teich, Multiphoton absorption cross section and virtual-state spectroscopy for the entangled  $n$ -photon state, *Phys. Rev. A* **57**, 3972 (1998).
- [50] B. E. A. Saleh, A. Joobeur, and M. C. Teich, Spatial effects in two- and four-beam interference of partially entangled biphotons, *Phys. Rev. A* **57**, 3991 (1998).
- [51] R. de J León-Montiel, J. Svozilík, L. J. Salazar-Serrano, and J. P. Torres, Role of the spectral shape of quantum correlations in two-photon virtual-state spectroscopy, *New Journal of Physics* **15**, 053023 (2013).
- [52] F. Schlawin and A. Buchleitner, Theory of coherent control with quantum light, *New Journal of Physics* **19**, 013009 (2017).
- [53] E. G. Carnio, A. Buchleitner, and F. Schlawin, How to optimize the absorption of two entangled photons, *SciPost Phys. Core* **4**, 028 (2021).
- [54] B. R. Mollow, Two-photon absorption and field correlation functions, *Phys. Rev.* **175**, 1555 (1968).
- [55] F. Chen and S. Mukamel, Entangled two-photon absorption with Brownian-oscillator fluctuations, *The Journal of Chemical Physics* **156**, 074303 (2022).
- [56] M. G. Raymer, T. Landes, and A. H. Marcus, Entangled two-photon absorption by atoms and molecules: A quantum optics tutorial, *The Journal of Chemical Physics* **155**, 081501 (2021).
- [57] H. Oka, Selective two-photon excitation of a vibronic state by correlated photons, *The Journal of Chemical Physics* **134**, 124313 (2011).
- [58] H. Oka, Control of vibronic excitation using quantum-correlated photons, *The Journal of chemical physics* **135**, <https://doi.org/10.1063/1.3654136> (2011).
- [59] F. Lever, S. Ramelow, and M. Gühr, Effects of time-energy correlation strength in molecular entangled photon spectroscopy, *Phys. Rev. A* **100**, 053844 (2019).
- [60] F. Schlawin and S. Mukamel, Matter correlations induced by coupling to quantum light, *Phys. Rev. A* **89**, 013830 (2014).
- [61] O. Varnavski, S. K. Giri, T.-M. Chiang, C. J. Zeman IV, G. C. Schatz, and T. Goodson III, Colors of entangled two-photon absorption, *Proceedings of the National Academy of Sciences* **120**, e2307719120 (2023).
- [62] T. Landes, M. G. Raymer, M. Allgaier, S. Merkouche, B. J. Smith, and A. H. Marcus, Quantifying the enhancement of two-photon absorption due to spectral-temporal entanglement, *Opt. Express* **29**, 20022 (2021).
- [63] H. Oka, Enhanced and selective two-photon excitation of molecular vibronic states using entangled photons, *Photosynthetic Responses in Molecules and Molecular Aggregates*, **43** (2020).
- [64] H. Oka, Enhanced vibrational-mode-selective two-step excitation using ultrabroadband frequency-entangled photons, *Phys. Rev. A* **97**, 063859 (2018).
- [65] R. Loudon, *The quantum theory of light*, 3rd ed. (Oxford University Press, Oxford, 2000).
- [66] B. Dayan, Theory of two-photon interactions with broadband down-converted light and entangled photons, *Phys. Rev. A* **76**, 043813 (2007).
- [67] K. J. Blow, R. Loudon, S. J. D. Phoenix, and T. J. Shepherd, Continuum fields in quantum optics, *Phys. Rev. A* **42**, 4102 (1990).
- [68] D. J. Santos, R. Loudon, and F. J. Fraile-Peláez, Continuum states and fields in quantum optics, *American Journal of Physics* **65**, 126 (1997).
- [69] A. Migdall, S. V. Polyakov, J. Fan, and J. C. Bienfang, *Single-photon generation and detection: physics and applications* (Academic Press, 2013).
- [70] M. H. Rubin, D. N. Klyshko, Y. H. Shih, and A. V. Sergienko, Theory of two-photon entanglement in type-ii optical parametric down-conversion, *Phys. Rev. A* **50**, 5122 (1994).
- [71] A. V. Sergienko, Y. H. Shih, and M. H. Rubin, Experimental evaluation of a two-photon wave packet in type-ii parametric downconversion, *J. Opt. Soc. Am. B* **12**, 859 (1995).
- [72] C. K. Hong, Z. Y. Ou, and L. Mandel, Measurement of subpicosecond time intervals between two photons by interference, *Phys. Rev. Lett.* **59**, 2044 (1987).
- [73] Y. H. Shih, A. V. Sergienko, M. H. Rubin, T. E. Kiess, and C. O. Alley, Two-photon entanglement in type-ii parametric down-conversion, *Phys. Rev. A* **50**, 23 (1994).
- [74] B. Gu, S. Sun, F. Chen, and S. Mukamel, Photoelectron spectroscopy with entangled photons; enhanced spectrottemporal resolution, *Proceedings of the National Academy of Sciences* **120**, e2300541120 (2023).
- [75] A. Ekert and P. L. Knight, Entangled quantum systems and the Schmidt decomposition, *American Journal of Physics* **63**, 415 (1995).
- [76] A. Acín, A. Andrianov, L. Costa, E. Jané, J. I. Latorre, and R. Tarrach, Generalized schmidt decomposition and classification of three-quantum-bit states, *Phys. Rev. Lett.* **85**, 1560 (2000).
- [77] J. Sperling and W. Vogel, The schmidt number as a universal entanglement measure, *Physica Scripta* **83**, 045002 (2011).
- [78] C. K. Law, I. A. Walmsley, and J. H. Eberly, Continuous frequency entanglement: Effective finite hilbert space and entropy control, *Phys. Rev. Lett.* **84**, 5304 (2000).
- [79] M. E. Carrington, R. Kobes, G. Kunstatter, D. Ostapchuk, and G. Passante, Geometric measures of entanglement and the

- schmidt decomposition, *Journal of Physics A: Mathematical and Theoretical* **43**, 315302 (2010).
- [80] M. Fedorov and N. Miklin, Schmidt modes and entanglement, *Contemporary Physics* **55**, 94 (2014).
- [81] P. M. Morse, Diatomic molecules according to the wave mechanics. ii. vibrational levels, *Phys. Rev.* **34**, 57 (1929).
- [82] N. Rosen and P. M. Morse, On the vibrations of polyatomic molecules, *Phys. Rev.* **42**, 210 (1932).
- [83] T. E. Sharp and H. M. Rosenstock, Franck—Condon Factors for Polyatomic Molecules, *The Journal of Chemical Physics* **41**, 3453 (1964).
- [84] T. Baumert, M. Grosser, R. Thalweiser, and G. Gerber, Femtosecond time-resolved molecular multiphoton ionization: The  $\text{Na}_2$  system, *Phys. Rev. Lett.* **67**, 3753 (1991).
- [85] S. Magnier, P. Millié, O. Dulieu, and F. Masnou-Seeuws, Potential curves for the ground and excited states of the  $\text{Na}_2$  molecule up to the  $(3s+5p)$  dissociation limit: Results of two different effective potential calculations, *The Journal of Chemical Physics* **98**, 7113 (1993).
- [86] J. P. Zayner and T. R. Sosnick, Factors that control the chemistry of the lov domain photocycle, *PloS one* **9**, e87074 (2014).
- [87] F. Lindner and A. Diepold, Optogenetics in bacteria—applications and opportunities, *FEMS Microbiology Reviews* **46**, fuab055 (2022).
- [88] A. Losi, K. H. Gardner, and A. Möglich, Blue-light receptors for optogenetics, *Chemical reviews* **118**, 10659 (2018).
- [89] S. Kundu, P. P. Roy, G. R. Fleming, and N. Makri, Franck—condon and herzberg—teller signatures in molecular absorption and emission spectra, *The Journal of Physical Chemistry B* **126**, 2899 (2022), pMID: 35389662.
- [90] P. P. Roy, S. Kundu, N. Makri, and G. R. Fleming, Interference between franck—condon and herzberg—teller terms in the condensed-phase molecular spectra of metal-based tetrapyrrole derivatives, *The Journal of Physical Chemistry Letters* **13**, 7413 (2022), pMID: 35929598.
- [91] Y. Qian, X. Li, A. R. Harutyunyan, G. Chen, Y. Rao, and H. Chen, Herzberg—teller effect on the vibrationally resolved absorption spectra of single-crystalline pentacene at finite temperatures, *The Journal of Physical Chemistry A* **124**, 9156 (2020), pMID: 33103890.
- [92] H. Oka, Highly-efficient entangled two-photon absorption with the assistance of plasmon nanoantenna, *Journal of Physics B: Atomic, Molecular and Optical Physics* **48**, 115503 (2015).
- [93] H. Oka, Generation of broadband ultraviolet frequency-entangled photons using cavity quantum plasmonics, *Scientific Reports* **7**, 8047 (2017).
- [94] H. Oka, Generation of broadband frequency-entangled photons using plasmon nanoantenna, *Applied Physics Letters* **103**, <https://doi.org/10.1063/1.4826646> (2013).
- [95] E. Rusak, J. Straubel, P. Gladysz, M. Göddel, A. Kedziorski, M. Kühn, F. Weigend, C. Rockstuhl, and K. Slowik, Enhancement of and interference among higher order multipole transitions in molecules near a plasmonic nanoantenna, *Nature communications* **10**, 5775 (2019).
- [96] S. I. Jahromi and K. Slowik, Multiphoton absorption enhancement by graphene—gold nanostructure, *Opt. Lett.* **49**, 3914 (2024).
- [97] S. Izadshenas and K. Slowik, Molecular saturation determines distinct plasmonic enhancement scenarios for two-photon absorption signal, arXiv preprint arXiv:2408.14859 <https://doi.org/10.48550/arXiv.2408.14859> (2024).